

Quantum states in fractional dimension: long-range entanglement and self-similarity

Wei Wang (王巍)^{1,*}

¹ *Tsung-Dao Lee Institute, Shanghai Jiao Tong University, Shanghai, 201210, China*

Quantum matter with fractal geometry has been recently realized in experiments. Fundamentally distinctive properties in such new type of matter, e.g., the fractional spatial dimension between 1D and 2D, signify novel quantum order lying beyond paradigms developed in integer dimensions. Following the perspective that quantum orders are encoded in entanglement patterns, we reveal such novelty by studying the interplay between entanglement and fractal self-similarity as realized in renormalization fixed points. In particular, we prove the coexistence between long-range entanglement and fractality in a fixed-point state that has zero correlation length but cannot be completely disentangled by constant-depth local quantum circuits. We show that our example reveals the existence of a new paradigm of realizing long-range entanglement in addition to the picture of topological order, and hence evidences novel quantum order inherent in fractional dimension. Examples of fixed points in this work are generated within a framework based on tensor network which can be applied to a wide class of geometries in fractional dimensions for studying nontrivial entanglement patterns. Based on our work, new study on the connection between quantum matter and quantum information is expected.

I. INTRODUCTION

Quantum order characterizes the quantum origin of correlated ground states belonging to a quantum phase. Discovering novel quantum order keeps refreshing our understanding of quantum emergent phenomena and building the bridge between quantum information and quantum matter. A famous example is the discovery of topological order in 2D, which lies beyond the Ginzburg-Landau paradigm [1–3] and provides a foundation for topological quantum computation [4, 5].

Recent experimental realizations of quantum many-body systems with fractal geometry have revealed a new type of quantum matter [6–10]. In such systems, regularity and periodicity disappear while self-similarity shapes the locality and the scaling, and determines the fractional spatial dimension between 1D and 2D. These distinctions endow fractal quantum matter with intrinsically different properties from those in integer dimensions. Motivated by such distinctions, theoretical studies initially focused on adjusting the paradigm of 2D topological quantum phases to fractal geometry [11–23]. However, in extending the topological picture to fractional dimension [24], certain fundamental incompatibility eventually draws attention to the existence of novel quantum order which lies beyond paradigms developed in integer dimensions and might provide new connection between quantum information and quantum matter.

It is a challenge to capture such novelty in fractal quantum matter, since the reliability of many theoretical tools developed in integer dimensions is undermined. For example in the famous Sierpiński fractal with fractional dimension 1.58 (see Fig. 1(a)), geometric concepts like bulk and boundary cannot be well-defined since any region claimed as bulk contains region inside which can be

claimed as boundary. Consequently, numerical study of lattice models based on such concepts can lead to ambiguity in conclusion.

To reveal the novelty within a general framework and on a reliable basis, we consider concrete examples of quantum states and follow the quantum-information perspective on quantum order: Quantum orders are encoded in distinct entanglement patterns of quantum states which can be read off the lattice locality [25, 26]. In other words, entanglement pattern of a state portrays the low energy physics of a model that can stabilize the state as a ground state. 2D topological order, again, provides a prominent example where topological features and anyonic excitations emerge out of global “dancing” patterns of entangled local degrees of freedom in the ground state, i.e. long-range entanglement patterns [4, 25–29]. This entanglement perspective bridges quantum matter and quantum information, and validates the study of quantum order directly from quantum states without resorting to a specific Hamiltonian. Indeed, in realizing long-range entangled states and the braiding statistics of anyons emergent thereon, both experimental approaches with [30] and without [31] a specific Hamiltonian have been recently demonstrated.

In this work, we study nontrivial patterns [32] in entanglement-renormalization fixed-point states of qudit (\mathbb{C}^d , or equivalently spin) systems on fractal lattice. For simplicity, we consider qudits on the Sierpiński lattice which has attracted most attention in experiments [6–10]. Our basic consideration is that fixed points with zero correlation length possess the “cleanest” entanglement patterns to represent quantum order since the short-range part of entanglement is washed out as much as possible in the renormalization flow [33, 34]. We show that the fixed-point states possess well-defined self-similarity in their entanglement which realize the interplay between entanglement and fractal self-similarity. Based on such interplay, we study how nonlocal information is encoded in the fixed-point states and capture the novelty of quan-

* wwwwei-wwwwang@sjtu.edu.cn

tum order therein.

The central part of our work is the proof of long-range entanglement (LRE) in one example of fixed-point state. Here, LRE refers to the entanglement in a state which has short-range correlation but cannot be completely disentangled through constant-depth local quantum circuit. Note that in 2D, it is such paradoxical combination of the absent correlation and the nonlocally encoded information which reveals LRE as emergent topological order with anyonic excitations and gives rise to the topological entanglement entropy [4, 25, 26, 35, 36]. This combination distinguishes LRE from the Greenberger-Horne-Zeilinger-type (GHZ-type) entanglement patterns and those harboring long-range order [26]. It has also attracted great attention in experimental studies for the application in quantum computation [30, 31, 37, 38]. Indeed, the correlation and the quantum-circuit arguments only require a lattice or a graph structure to specify the locality properties about the adjacency of vertices so that the existence of LRE can be studied in any dimension [39]. Nevertheless, whether LRE exists or not, and how it gives rise to emergent properties depend on spatial dimensions, since the manner that nonlocal information is encoded depends on locality properties that are intrinsically different in different dimensions. For example, LRE does not exist in 1D since the combination defining LRE contradicts the locality properties of 1D systems [26]. Even in 2D, it is still not proved whether topological order is the only paradigm for realizing LRE. In general, these facts make LRE a symbol of highly non-trivial quantum order. In this work, our example not only proves the coexistence between LRE and fractality in fractional dimension, but also reveals the existence of a new paradigm for realizing LRE in addition to the picture of topological order.

The main body of this manuscript is the study on the entanglement and self-similarity properties of fixed points. We also introduce toy models of strongly interacting hardcore bosons which stabilize the fixed points as ground states, and might shed light on searching for experimentally realizable models. All fixed points in our work are generated as solutions to a scale-invariance equation within a framework based on tensor network, which can be generalized to a wide class of fractal systems. The rest of the paper is organized as follows. In Sec. II and III, we introduce the framework and establish the equivalence between the fixed-point scale invariance and the self-similarity in entanglement. To illustrate the framework, we give a simple example of fixed point possessing infinite correlation length and 2D chirality in Sec. IV. Then, we study a fixed-point state of short-range entanglement (SRE) by solving a toy model in Sec. V. While the first two examples demonstrate different schemes of self-similarity in entanglement, they can also be viewed as preparation for the study of the fixed-point state with LRE in Sec. VI, the core of our study. In Sec. VI we spend two subsections on the proof for LRE, i.e., on the zero correlation length and the quan-

tum circuit arguments respectively; we then explain why the LRE in our example lies beyond the paradigm of topological order; and we end our discussion with a toy model which effectively stabilizes the fixed point as a unique ground state.

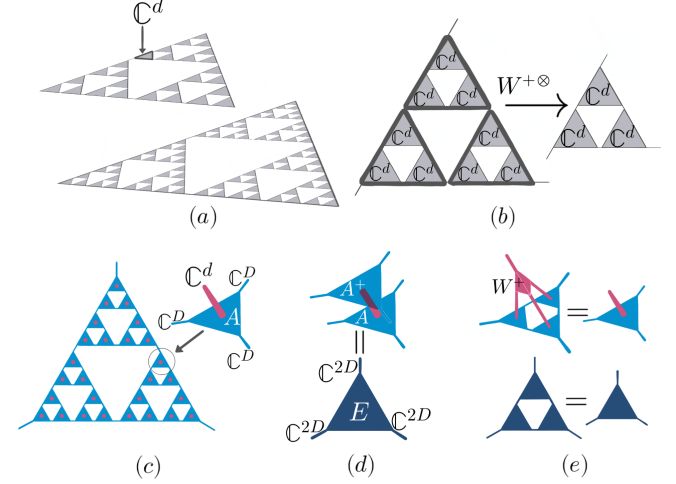


FIG. 1. (a) Qudit system on the Sierpiński lattices in different sizes. (b) The blocks of qudits and the coarse graining operation. (c) The tensor network formed by copies of the tensor A . The red leg represents the physical index while the blue represent virtual indices. (d) The definition of transfer matrix E from A . (e) The two equivalent scale-invariance equations for contracting copies of A and of E respectively.

II. ENTANGLEMENT-RENORMALIZATION FIXED POINTS

Our framework for entanglement renormalization is essentially a scheme of wavefunction renormalization, which do not resort to local Hamiltonians but parameterizes quantum states with tensors. We define the coarse graining operation which generates renormalization flow as shown in Fig. 1(b). It is an operator $(W^+)^{\otimes(N/3)}$ which maps N qudits into $N/3$ qudits in a larger scale but with the same lattice geometry. In general, the isometry $W : \mathbb{C}^d \rightarrow \mathbb{C}^{d^3}$ is defined in terms of the state in the renormalization flow so that $W^+ : \mathbb{C}^{d^3} \rightarrow \mathbb{C}^d$ (see Fig. 1(b)) extracts exactly the degrees of freedom that is in charge of the entanglement between one qudit block and its neighboring blocks. Following the spirit of the infinite-tensor-network ansatz [33, 40–42], we represent a fixed-point state $|\Psi\rangle$ on the infinite Sierpiński lattice as contracted from infinite copies of a single (or a finite number of) tensor $A = \sum_{\alpha\beta\beta'\beta''} A(\alpha\beta\beta'\beta'') |\alpha\beta\beta'\beta''\rangle \in \mathbb{C}^d \otimes \mathbb{C}^{d^3}$ as shown in Fig. 1(c). Here $|\alpha\rangle \in \mathbb{C}^d$ is the physical index representing the local degrees of freedom, and $|\beta\rangle, |\beta'\rangle, |\beta''\rangle \in \mathbb{C}^d$ are virtual indices resembling the linking between nearest neighboring vertices. The fixed-point states are simply solutions to the scale-invariance

equation of the coarse graining $(W^+)^{\otimes}$. In our setup, the equation is

$$W^+ \text{Tr}_{\{\mathbb{C}^D\}}[A \otimes A \otimes A] = \lambda A, \quad (1)$$

where the contraction on each block of three copies of A followed by W^+ results in A itself times a constant λ , and hence $|\Psi\rangle$ as represented by the tensor is invariant (see Fig. 1(e)). Note that in cases where $|\Psi\rangle$ is determined by multiple tensors, there are correspondingly more than one scale-invariance equations as will be shown in example.

Strictly speaking, state on infinite lattice is not well-defined. However, we can define states $|\Psi\rangle_n$ on the n th-finite-generation of the Sierpiński lattice as contracted from finite copies of A (see Fig. 1(c)) together with three constant corner tensors $C_1 = \sum_{\beta_1} C(\beta_1) |\beta_1\rangle, C_2 = \sum_{\beta_2} C(\beta_2) |\beta_2\rangle, C_3 = \sum_{\beta_3} C(\beta_3) |\beta_3\rangle$ (with no physical index and independent on the system size) on the three outermost virtual indices $\beta_1, \beta_2, \beta_3$. Then, when identifying $|\Psi\rangle_n$ and $W^{+\otimes} |\Psi\rangle_n \propto |\Psi\rangle_{n-1}$ for scale invariance, we can only focus on copies from the tensor A as if working on the infinite case. Indeed, we can go to arbitrarily large n in order to avoid directly working on infinite lattice but grasp the scale invariance in the entanglement which will be shown in examples. In this way, we can safely speak of $|\Psi\rangle$ as contracted from infinite copies of A . In the following, $|\Psi\rangle$ is understood either as the state at an arbitrary finite system size or the state at infinite system size, depending on the context.

III. SELF-SIMILARITY IN ENTANGLEMENT

Eq. 1 ensures certain self-similar structure in the entanglement of $|\Psi\rangle$. Indeed, while the three virtual legs of A represent the entanglement between one qudit and its neighbors, $\text{Tr}_{\{\mathbb{C}^D\}}[A \otimes A \otimes A]$ also has three virtual legs which similarly represent the entanglement between one block of qudits and its neighboring blocks (see Fig. 1(c), 1(e)). Then, since W^+ only removes entanglement inside each block, just like how the zoom-out operation replace each block by a vertex (or W resembling the reverse operation), the equality in Eq. 1 implies that blocks of qudits are entangled in the same way as qudits are entangled, i.e. the entanglement in $|\Psi\rangle$ has zoom-in and zoom-out invariance, or equivalently, self-similarity. This argument can be formalized with the transfer matrix $\mathbf{E} = A^+ A$ [43] (see Fig. 1(d)) as discussed in App. A 1. In short, characterization of a fixed-point state including both the tensor A and the coarse graining operator W can be uniquely specified solely from a \mathbf{E} with an equivalent scale invariance equation $\text{Tr}_{\{\mathbb{C}^{2D}\}}[\mathbf{E} \otimes \mathbf{E} \otimes \mathbf{E}] = |\lambda|^2 \mathbf{E}$ which does not explicitly include W but fully captures the zoom-in and the zoom-out invariance (see Fig. 1(e)). In other words, a fixed-point state is exactly a realization of the interplay between entanglement and self-similarity.

Our framework establishes the identity between the scale invariance of $|\Psi\rangle$ and the fractal self-similarity in

the entanglement of $|\Psi\rangle$ which distinguishes from integer dimensions. Firstly, our scale-invariance equation distinguishes from that in the tensor-network representation in 2D where further operations on virtual indices following the coarse graining operator, e.g., removal of indices, is required to keep the lattice geometry [26]. Then in 1D, while the lattice geometry is also preserved by the coarse graining operator [33], fractal geometry harbors essentially different physics from those in 1D, e.g., numerical evidence of anyon braiding [15] which does not exist in 1D. These apparent distinctions are all encoded in the entanglement patterns intrinsic to the spatial dimensions respectively. Therefore, as will be further demonstrated in examples, non-triviality and novelty in quantum order of fractal quantum matter emerge from nontrivial interplay between self-similarity and entanglement properties as given by solutions to Eq. 1.

IV. CHIRALITY AND INFINITE CORRELATION LENGTH

Before studying fixed points with zero correlation length, we firstly give a simple solution to Eq. 1 to illustrate the above framework and the meaning of entanglement pattern. This example has infinite correlation length, and is a realization of the compatibility between self-similarity and 2D-chirality.

The tensor A consists of the physical index as $|\alpha\rangle = |1\rangle, \dots, |6\rangle \in \mathbb{C}^6$ and three virtual indices given by $|\beta\rangle = |a\rangle, |b\rangle, |c\rangle \in \mathbb{C}^3$. We specify A by listing the nonzero elements of $A(\alpha\beta'\beta'')$ which are all equal to 1 in Fig. 2(a). In contracting copies of A , we always take the convention that the top of each copy of tensor inside a block is outward (Fig. 2(a)). The contraction of copies of A together with the constant corner tensors $C_1 = \sum_{\beta_1} |\beta_1\rangle, C_2 = \sum_{\beta_2} |\beta_2\rangle, C_3 = \sum_{\beta_3} |\beta_3\rangle$ gives the fixed-point state $|\Psi\rangle = 1/\sqrt{6} \sum_{m=1}^6 |\psi_m\rangle$ (up to the normalizer). Indeed, according to the illustration of non-vanishing contraction in Fig. 2(a), the qudit-product-state $|\psi_m\rangle$ of the form $|\alpha\alpha'\alpha''\dots\rangle$ is specified by the constraints (see Fig. 2(b)): In each $|\psi_m\rangle$ the configuration of qudits within each block can only be $\begin{smallmatrix} 1 & 3 & 5 & 2 \\ 3 & 5 & 1 & 1 \\ 3 & 5 & 1 & 1 \\ 6 & 4 \end{smallmatrix}$, $\begin{smallmatrix} 4 & 6 \\ 2 & 6 \end{smallmatrix}$ or $\begin{smallmatrix} 6 \\ 4 & 2 \end{smallmatrix}$; and single-qudit states on neighboring vertices linking two blocks are identical. Then, the constant corner tensors sum $|\psi_m\rangle$'s with equal weight to $|\Psi\rangle$. The constraints characterize the entanglement pattern of $|\Psi\rangle$ as shown pictorially in Fig. 2(b). According to the constraints, the state of one qudit exactly determines that of another arbitrarily distant qudit, giving rise to infinite correlation length.

The self-similarity or the scale invariance of $|\Psi\rangle$ can be

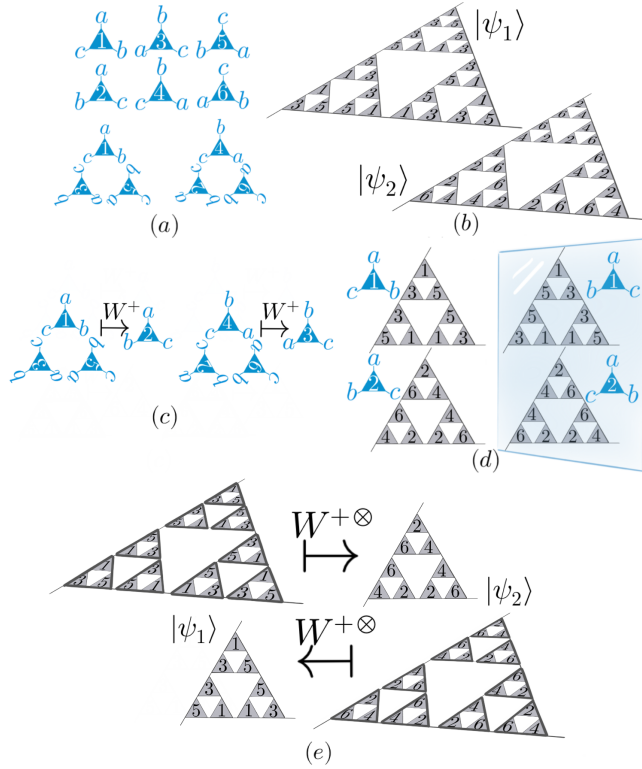


FIG. 2. (a) Nonzero elements of $A(\alpha\beta\beta'\beta'')$ which are all equal to 1 (upper). The convention of orientation for contraction (lower). (b) $|\psi_1\rangle$ and $|\psi_2\rangle$. $|\psi_3\rangle$ ($|\psi_4\rangle$) and $|\psi_5\rangle$ ($|\psi_6\rangle$) can be obtained by rotating $|\psi_1\rangle$ ($|\psi_2\rangle$) clockwise (counterclockwise) through $2\pi/3$ and $4\pi/3$ respectively. (c) W^+ acted on $\text{Tr}_{\{C^D\}}[A \otimes A \otimes A]$. (d) The mirror image of A and $\{|\psi_m\rangle\}$ is obtained by exchanging the odd states and the even states in the physical index of A or equivalently switching the configuration in a block of $|\psi_m\rangle$ between being clockwise and being counterclockwise. (e) $(W^+)^{\otimes}$ maps $|\psi_1\rangle$ to $|\psi_2\rangle$ (in a larger scale) and maps $|\psi_2\rangle$ to $|\psi_1\rangle$.

shown with the coarse graining operator defined as

$$W^+ = \left| 2 \right\rangle \left\langle \begin{array}{c} 1 \\ 3 \ 5 \end{array} \right| + \left| 4 \right\rangle \left\langle \begin{array}{c} 3 \\ 5 \ 1 \end{array} \right| + \left| 6 \right\rangle \left\langle \begin{array}{c} 5 \\ 1 \ 3 \end{array} \right| + \left| 1 \right\rangle \left\langle \begin{array}{c} 2 \\ 6 \ 4 \end{array} \right| + \left| 3 \right\rangle \left\langle \begin{array}{c} 4 \\ 2 \ 6 \end{array} \right| + \left| 5 \right\rangle \left\langle \begin{array}{c} 6 \\ 4 \ 2 \end{array} \right|$$

(see Fig. 2(c) and 2(e)), which makes A a solution to Eq. 1 and keeps the constraints specifying $|\psi_m\rangle$ unchanged. Indeed as illustrated in Fig. 2(e), $(W^+)^{\otimes}$ maps $|\psi_1\rangle + |\psi_3\rangle + |\psi_5\rangle$ and $|\psi_2\rangle + |\psi_4\rangle + |\psi_6\rangle$ to each other (in a large scale), hence maps $|\Psi\rangle$ to itself. Note that $|\psi_1\rangle + |\psi_3\rangle + |\psi_5\rangle$ or $|\psi_2\rangle + |\psi_4\rangle + |\psi_6\rangle$ does not possess the self-similarity individually. The invariance of the constraints under the coarse graining characterizes the self-similarity of $|\Psi\rangle$, and also the interplay between self-similarity and entanglement realized in $|\Psi\rangle$. Note that when applying $(W^+)^{\otimes}$, we always take the convention that the three-qudit-state configuration in a block or in $\text{Tr}_{\{C^D\}}[A \otimes A \otimes A]$ is read as if the top of the configuration is the outermost in the larger block (see Fig. 2(c) and

2(e)). Fig. 2(d) gives the mirror image A' and $|\psi'_m\rangle$, and hence $|\Psi'\rangle$. Obviously, $\{|\psi'_m\rangle\}$ form a representation of rotational symmetry which is orthogonal to that formed from $\{|\psi_m\rangle\}$. Therefore, $|\Psi\rangle$ is 2D-chiral, i.e. $|\Psi'\rangle$ cannot be superimposed with $|\Psi\rangle$ through 2D translation or rotation.

V. SHORT-RANGE ENTANGLEMENT PATTERN (SRE)

Now we study fixed-point states in which short-range correlation is completely washed out through the coarse graining, but certain genuine multipartite entanglement still remains. As a prelude for describing long-range entanglement pattern and corresponding model, we start with an example of short-range entanglement pattern (SRE). To emphasize that Eq. 1 can give rise to ground states of interacting bosons, we firstly introduce the model and then show how its ground state is represented by the solution to Eq. 1.

A. Toy model of trilayer hardcore bosons

In this case, a qudit can be decomposed into individual degrees of freedom corresponding to the entanglement between the qudit and its different neighbors. We can effectively realize the fixed point as the ground state in a model of trilayer-lattice (with Sierpiński geometry and label $s = 1, 2, 3$) hardcore boson system. Then, a basis of the qudit $|\alpha\rangle \in \mathbb{C}^8$, $\alpha = 1, \dots, 8$ on a vertex is identified with $|x_1 x_2 x_3\rangle$, $x_s = 0, 1$ for occupations on the same vertex but in different layers, i.e. the individual degrees of freedom (see Fig. 3(a)). The Hamiltonian is

$$H = -t \sum_{(k,l)} (a_{-k}^1 a_l^1 + a_{-k}^2 a_l^2 + a_{-k}^3 a_l^3) + \text{c.c.} + v \sum_{(i,j)} n_i^1 n_j^1 + v \sum_{(i,i',i'')} (n_i^2 n_{i'}^2 + n_{i'}^2 n_{i''}^2 + n_{i''}^2 n_i^2), \quad (2)$$

where $t, v > 0$; (k, l) is a pair of arbitrary nearest neighboring vertices; (i, j) is a pair of neighboring vertices linking two blocks; (i, i', i'') stands for the three vertices clockwise inside a block; and a_i^s ($a_i^{s\dagger}$) is annihilation (creation) operator with $n_i^s = a_i^{s\dagger} a_i^s$ (see Fig. 3(a)). Bosons on layer-1 have intralayer hopping on nearest neighbors and repulsive intralayer interaction on vertices linking two blocks; bosons on layer-2 and layer-3 have interlayer hopping on nearest neighbors and repulsive interlayer interactions on vertices inside each block (see Fig. 3(a)).

Note that we choose the model with Bose-Hubbard-type hopping terms and repulsive interaction instead of even simpler alternatives, because the general Bose-Hubbard-type models can be simulated in different experimental settings with high controllability in both spatial geometry and forms of boson-boson coupling [44, 45].

However, as a Hamiltonian stabilizing renormalization fixed point, H may differ from usually studied Bose-Hubbard-type models in the terms corresponding to the washed-out correlations. We expect that more realistic models with hopping and interaction terms modified accordingly can stabilize states flowing to the fixed-point state studied here.

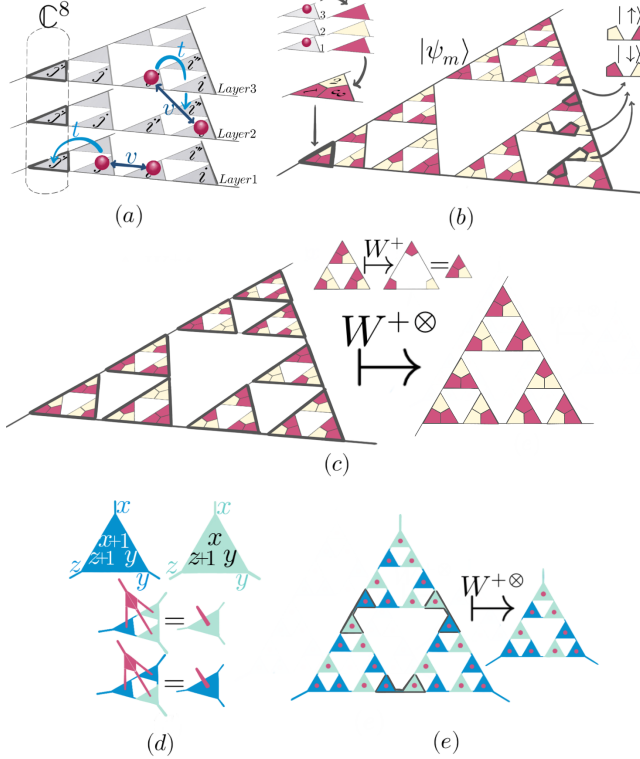


FIG. 3. (a) The trilayer hardcore boson system, effective local qudit, the hopping and the interaction terms. (b) $|\psi_m\rangle$ as qudit-product state of the form $|\alpha\alpha'\alpha''\dots\rangle$ where each $|\alpha\rangle$ ($|x_1x_2x_3\rangle$) is represented by a triangle of yellow ($x = 0$) and red ($x = 1$) colors. A red-yellow (yellow-red) pair can be viewed as $|\uparrow\rangle_{n'} \langle \downarrow|_{n'}$ of a 1/2-spin on a link n' of the lattice. (c) The coarse graining on $|\psi_m\rangle$. (d) Nonzero elements in tensor A_0 (dark blue), A_1 (light green) which are equal to 1. $x, y, z \in \mathbb{Z}_2$. And the scale-invariance equations for the two tensors. (e) The tensor-network representation of $|\Psi\rangle$ and the coarse graining on the tensor network. The bold lines circulate the six copies of tensors at the three inward corners linking three (big) block triangles inside a larger block triangle.

We fix the filling factor for each layer as $N^1/N = 1/2, (N^2 + N^3)/N = 1$ [46] ($N^s = \sum_i n_i^s, s = 1, 2, 3$ and N the number of vertices in one layer) and solve this model in the strong-interaction limit $t \ll v$ by treating the hopping H_1 as a perturbation to the interaction H_0 . Due to the interaction energy gap, the physics of the system is captured by an effective Hamiltonian H_{eff} within the subspace $\mathcal{H}_0 \subset \mathbb{C}^{8 \otimes N}$ spanned by qudit-product-states $|\psi_m\rangle$ with the lowest interaction energy. According to the perturbation theory [29], H_{eff} is sim-

ply the lowest-order non-vanishing term in the sequence $P(H_1 + H_1 G'_0 H_1 + H_1 G'_0 H_1 G'_0 H_1 + \dots)P$ where G'_0 is the unperturbed Green function for H_0 acting only on excited states (of H_0), and $P = \sum_m |\psi_m\rangle \langle \psi_m|$ is the projection onto \mathcal{H}_0 .

Minimizing the repulsive interaction energy specifies $|\psi_m\rangle$ (of the form $|\alpha\alpha'\alpha''\dots\rangle$) as determined by the following constraints: For a pair of neighboring vertices linking two blocks, the qudit states are $|x_1x_2x_3\rangle$ and $|(x_1+1)y_2y_3\rangle$; inside a block, the three-qudit-state configuration is clockwise ($|x_1x_2(z_2+1)\rangle, |y_1y_2(x_2+1)\rangle, |z_1z_2(y_2+1)\rangle$). Here, we use $x, y, z = 0, 1 \in \mathbb{Z}_2$, i.e. $1+1 = 0, 0+1 = 1$. To illustrate the constraints, we represent each single-qudit state $|\alpha\rangle$ ($|x_1x_2x_3\rangle$) by a colored triangle with x_1, x_2, x_3 clockwise being assigned the color red ($=1$) or yellow ($=0$) (see Fig. 3(b)). In arranging those triangles ($|\alpha\rangle$) to represent $|\psi_m\rangle$ ($|\alpha\alpha'\alpha''\dots\rangle$), we take the convention that the color for x_1 in each triangle is the outermost piece in a block. This way, the constraints as illustrated in Fig. 3(b) simply read as: the pair of neighboring colors linking two neighboring triangles (vertices) are opposite. As shown in Fig. 3(b), a red-yellow (yellow-red) pair can be viewed as $|\uparrow\rangle_{n'} \langle \downarrow|_{n'}$ of a 1/2-spin on a link n' of the lattice. These pairs are independent and cover all local degrees of freedom except for the corners. Consequently, a $|\psi_m\rangle$ can be identified with $|\uparrow\downarrow\dots\uparrow\rangle$ up to the occupation x_1 in the three corner qudits of the finite lattice which are not engaged in the interaction (see Fig. 3(b)). In this way, non-vanishing terms in PH_1P are hopping terms or equivalently σ_n^x 's which exchange the red-yellow and yellow-red pairs while leaving the x_1 's in the corner qudits unchanged.

As a result, \mathcal{H}_0 has 8 sectors (the 8 choices of the occupation x_1 of the three corner qudits) and each of the sector is isomorphic to $(\mathbb{C}^2)^{\otimes N'}$ (N' the number of links of the finite Sierpiński lattice). H_{eff} is invariant within each sector and has the equivalent form $-\sum_{n'} \sigma_n^x$, describing uncoupled spins located on links of the lattice. Hence, the system is exactly solvable with 8-fold-degenerate gapped ground states each of which has the form $|\Psi\rangle = 1/\sqrt{2^{N'}} \sum_m |\psi_m\rangle$, i.e. the equal-weight sum of all $|\psi_m\rangle$ in a sector, or equivalently the state $\otimes_{n'} (|\uparrow\rangle_{n'} + |\downarrow\rangle_{n'})$ of 1/2-spins. Obviously, adding local terms (fixing the x_1) on the corner qudits to H can remove the degeneracy, hence we consider $|\Psi\rangle$ as the unique ground state (specified by the local terms added).

B. Self-similarity and valence-bond-type entanglement

The self-similarity or the scale invariance of $|\Psi\rangle$ can be shown with the coarse graining operator

$$W^+ = \frac{1}{\sqrt{8}} \sum_{x_1, y_1, z_1 \in \mathbb{Z}_2} \sum_{x_2, y_2, z_2 \in \mathbb{Z}_2} |x_1 y_1 z_1 \langle x_1 x_2 (z_2 + 1), y_1 y_2 (x_2 + 1), z_1 z_2 (y_2 + 1)|.$$

In the illustration in Fig. 3(c), W^+ acts on $|\psi_m\rangle$ to remove the degrees of freedom on occupation x_2 and x_3 inside each block and only keeps the x_1 at each corner of a block. Because each pair of colors on x_1 that links neighboring blocks is opposite, the remaining x_1 's in each block form a new $|\alpha\rangle$ in some $|\psi_{m'}\rangle$ (in a larger scale) which satisfies the same constraints. Consequently, $|\Psi\rangle$ as the equal-weight sum of $|\psi_m\rangle$ is scale invariant.

As illustrated in Fig. 3(d), the tensor-network representation of $|\Psi\rangle$ is given by copies of two tensors A_0 and A_1 satisfying the scale-invariance equations with W^+ . They have physical index the same as $|\alpha\rangle = |xyz\rangle \in \mathbb{C}^8$ for $x, y, z = 0, 1$ and virtual indices $|\beta\rangle = |0\rangle, |1\rangle \in \mathbb{C}^2$. In the contraction, copies of the two tensors appear in a fixed pattern which is invariant to the coarse graining (see Fig. 3(e)): A_0 and A_1 link two neighboring blocks (of arbitrary size); the six copies of tensors at the three inward corners linking three (big) block triangles inside a larger block triangle appears alternatively as $A_0, A_1, A_0, A_1, A_0, A_1$. The tensors A_0 and A_1 can be viewed as product states in $\mathbb{C}^{\sqrt[3]{d} \times D} \otimes \mathbb{C}^{\sqrt[3]{d} \times D} \otimes \mathbb{C}^{\sqrt[3]{d} \times D}$, e.g., $A_0 = |x+1, x\rangle \otimes |y, y\rangle \otimes |z+1, z\rangle$ (see Fig. 3(d)), to guarantee the opposite-color constraints on the physical indices inside each block. And the pattern of A_0 and A_1 guarantees such constraints on all qubits. Then, constant corner tensors (chosen according to the local corner terms), e.g., $C_1, C_2, C_3 = |1\rangle$, contracted with copies of A_0 and A_1 , resulting in $|\Psi\rangle$. Note that due to the fractal geometry, copies of a single tensor cannot give the ground state.

The invariance of the constraints as pictorially shown in Fig. 3(b) and 3(c) characterizes the interplay between self-similarity and the entanglement pattern of $|\Psi\rangle$. Indeed, $|\Psi\rangle$ possesses valence-bond type of entanglement where the independent pairs of opposite colors (the valence bonds) guarantees the genuine multipartite entanglement in $|\Psi\rangle$ and also determines its zero correlation length, i.e. two distant qudits not sharing a bond is not correlated. Similar to fixed points with valence-bond type of entanglement in 1D [26, 33], A_0 and A_1 are obviously injective tensors so that $|\Psi\rangle$ has SRE. Indeed, according to the study of symmetry-protected topological order (SPT) in integer dimensions [26, 33], states with different SPT orders, e.g., the Affleck-Kennedy-Lieb-Tasaki (AKLT) state of antiferromagnetic order [47], flow to the valence-bond-type fixed points in entanglement renormalizations similar to $|\Psi\rangle$. Hence, $|\Psi\rangle$ is expected

as a basis to generate different orders realizing the interplay between SPT and fractal self-similarity in fractional dimension, according to the projection operator acting on each qudit and realizing specific symmetry.

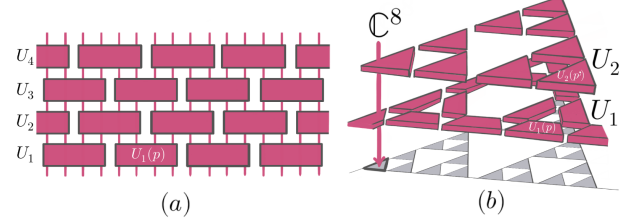


FIG. 4. (a) Local quantum circuit as layers of non-overlapping local unitary operators. The vertical lines stand for qudits and each rectangle is a local unitary operator. (b) Local quantum circuit $U_2 U_1$ for completely disentangling the $|\Psi\rangle$ with SRE.

C. Local quantum circuit

SRE is defined in terms of local quantum circuit. A local quantum circuit is a unitary operator $U = U_L \cdots U_2 U_1$. Here, each $U_l = \otimes_p U_l(p)$ is a product of unitary operators acting on nonoverlapping local patches $\{p\}$ of qudits with sizes smaller than some number P , and L is the depth of the circuit (see Fig. 4(a)). In the above example, $|\Psi\rangle$ can be completely disentangled through a quantum circuit U with $L = 2$ and $P = 3$ as shown in Fig. 4(b). In U_1 , each $U_1(p)$ acts on a pair of neighboring qudits linking two blocks, disentangling the color pairs ($|0x_2x_3\rangle \otimes |1y_2y_3\rangle \mapsto |0x_2x_3\rangle \otimes |1y_2y_3\rangle, |1x_2x_3\rangle \otimes |0y_2y_3\rangle \mapsto |1x_2x_3\rangle \otimes |1y_2y_3\rangle$) so that blocks of qudits are disentangled in $U_1|\Psi\rangle$. Then U_2 simply disentangle the three qudits within each block in a similar manner and hence completely disentangle $|\Psi\rangle$. In the quantum circuit U , the independence of L and P on the system size defines the SRE of $|\Psi\rangle$.

VI. LONG-RANGE ENTANGLEMENT PATTERN (LRE)

Based on the preparation from above examples, we now study the coexistence between LRE and fractality in a fixed-point state $|\Psi\rangle$, the core of our work. We start with the self-similarity in $|\Psi\rangle$ and prove that $|\Psi\rangle$ possesses LRE; then we explain why $|\Psi\rangle$ cannot be stabilized within the paradigm of (even extended) topological order by showing that the way nonlocal information encoded in $|\Psi\rangle$ is essentially different from that in any topologically ordered state; we end this study of LRE with a toy model which can effectively stabilize $|\Psi\rangle$ as the unique ground state.

Note that LRE in 2D can be probed by topological entanglement entropy (TEE) [35, 36] which represents the

LRE by a universal $-\gamma$ term (representing the nonlocal information encoded) added to the area law (reflecting the short-range correlation). However, as we have pointed out, the fractality is incompatible with the concepts bulk and boundary which underlie the meaning of the entanglement area law. Hence, the meaning of TEE in fractal geometry can only be developed based on proved states of LRE, instead of been used a priori.

In terms of the definition of SRE, LRE of a state $|\Psi\rangle$ is then defined by its short-range correlation and the dependence of the lower bounds of L and P on the system size for a local quantum circuit to completely disentangle $|\Psi\rangle$. In other words, a short-range correlated $|\Psi\rangle$ possesses LRE if and only if for arbitrarily given L and P , any local quantum circuit characterized by L and P cannot completely disentangle $|\Psi\rangle$ when the system is over certain size. Note that the characterization of LRE only requires a lattice or a graph structure to specify the locality properties of qudits about their adjacency, and hence can be studied in any spatial dimension.

A. Self-similarity in $|\Psi\rangle$

We now introduce the state $|\Psi\rangle$ as given by a tensor A , a solution to Eq. 1. Here, A still has the minimal nontrivial virtual index $|\beta\rangle = |0\rangle, |1\rangle \in \mathbb{C}^2$, but has the physical index $|\alpha\rangle = |0\rangle, |1\rangle, |2\rangle, |3\rangle \in \mathbb{C}^4$ so that A is not an injective tensor. We define the tensor

$$\begin{aligned} A &= A_0 + A_1 + A_2 + A_3, \\ A_0 &= |0\rangle \otimes |000 + 111\rangle, \quad A_1 = |1\rangle \otimes |100 + 011\rangle, \quad (3) \\ A_2 &= |2\rangle \otimes |010 + 101\rangle, \quad A_3 = |3\rangle \otimes |001 + 110\rangle, \end{aligned}$$

as illustrated in Fig. 5(a) where for convenience we represent $000 + 111$ by $\begin{smallmatrix} 1 & 1 & 1 \\ 0 & 0 & 0 \end{smallmatrix}$, $100 + 011$ by $\begin{smallmatrix} 0 & 1 & 1 \\ 1 & 0 & 0 \end{smallmatrix}$, etc.. According to this convenience, contraction of any three copies from A_0, A_1, A_2 and A_3 (following the convention introduced previously) does not vanish if and only if there are even number of flips between $\begin{smallmatrix} 1 & & \\ 0 & & \end{smallmatrix}$ and $\begin{smallmatrix} 0 & & \\ 1 & & \end{smallmatrix}$ along the circle formed by contracting indices (see Fig. 5(b)), or equivalently, there are even number of copies from A_2 or A_3 . It can be easily shown that such non-vanishing contraction in any finite size results in a tensor of the same form, e.g., the contraction of A_1, A_2, A_3 , as shown in Fig. 5(e), gives $|123\rangle \otimes \begin{smallmatrix} 0 & 1 & 1 \\ 1 & 0 & 0 \end{smallmatrix}$. Hence the condition for non-vanishing contraction (even number of flips) applies to all scales and determines the contraction of all the copies.

Copies of A together with constant corner tensors $C_1, C_2, C_3 = |1\rangle$ contracts into $|\Psi\rangle = 1/\sqrt{M} \sum_m |\psi_m\rangle$. Here, each qudit-product-states $|\psi_m\rangle$ of the form $|\alpha\alpha'\alpha''\cdots\rangle$ is specified by constraints originated from the above condition of non-vanishing contraction and the constant tensor, and M is the total number of such $|\psi_m\rangle$. The constraints specifying $|\psi_m\rangle$ can be elucidated pictorially by representing $|\psi_m\rangle$ in the following way (see Fig. 5(c)): We represent $|\alpha\rangle$'s by colored triangles with odd number of pink sides and even number of red

sides; in arranging those triangles ($|\alpha\rangle$) to represent $|\psi_m\rangle$ ($|\alpha\alpha'\alpha''\cdots\rangle$), we take the convention on the orientation of each triangles such that the triangle is outward in each block.

This way, the colored-triangle-representation of $|\alpha\rangle$'s are consistent with the definition of A_0, A_1, A_2 and A_3 , i.e., red sides corresponds to the pair of virtual indices with a flip between $\begin{smallmatrix} 1 & & \\ 0 & & \end{smallmatrix}$ and $\begin{smallmatrix} 0 & & \\ 1 & & \end{smallmatrix}$, the triangles and the tensors have the same convention of orientation. Then as shown in Fig. 5(c) and 5(d), because of the non-vanishing condition for contraction, there are constraints associated to each circle of vertices on which the colored sides form a closed chain or a ring; and the constraint on a circle is simply that the number of red sides in the ring is even. Moreover, according to the constant corner tensors, in finite size, such chain on each lateral side of the lattice as a big triangle has even number of red sides, i.e., only contractions of copies from A_0, A_1, A_2 and A_3 with the eventual form $|\{\alpha\}\rangle \otimes \begin{smallmatrix} 1 & 1 & 1 \\ 0 & 0 & 0 \end{smallmatrix}$ contribute to $|\Psi\rangle$. Note that in the infinite case, the constraints from the constant tensor are not important. The constraints guarantees the genuine multipartite entanglement in $|\Psi\rangle$, since any bipartition crosses circles with constraints. As is shown below, such constraints fully characterize the LRE pattern and its coexistence with fractal self-similarity.

Fig. 5(f) illustrates the self-similarity of $|\Psi\rangle$, i.e., the invariance of the constraints specifying $|\psi_m\rangle$ to the coarse graining. In the illustration, the coarse graining simply removes the inner sides of a block and only keeps the six outer sides which are eventually reduced into three sides according to the rule: two red (pink) sides on one side are reduced into one pink side; one red and one pink side are reduced into one red side. Formally, W^+ is defined as $1/\sqrt{8}$ times the sum

$$\begin{aligned} &|0\rangle\langle 000 + 111 + 023 + 132 + 213 + 230 + 302 + 321| \\ &+ |1\rangle\langle 011 + 032 + 100 + 123 + 202 + 221 + 313 + 330| \\ &+ |2\rangle\langle 010 + 033 + 101 + 122 + 203 + 220 + 312 + 331| \\ &+ |3\rangle\langle 001 + 110 + 022 + 133 + 212 + 231 + 303 + 320|. \end{aligned}$$

Here, each term in W^+ corresponds to a nonvanishing contraction of three copies from A_0, A_1, A_2, A_3 . For example, $|1\rangle\langle 123|$ corresponds to the contraction of A_1, A_2, A_3 (see Fig. 5(e)) which results in a tensor $|123\rangle \otimes \begin{smallmatrix} 0 & 1 & 1 \\ 1 & 0 & 0 \end{smallmatrix}$ that is eventually mapped to $A_1 = |1\rangle \otimes \begin{smallmatrix} 0 & 1 & 1 \\ 1 & 0 & 0 \end{smallmatrix}$ (up to a constant) through W^+ . Obviously, the tensor A together with W^+ satisfies Eq. 1.

B. Proof for the zero correlation length

To prove that $|\Psi\rangle$ possesses LRE, we firstly prove that $|\Psi\rangle$ has zero correlation length, i.e. $\langle \Psi | O_j O_i | \Psi \rangle - \langle \Psi | O_j | \Psi \rangle \langle \Psi | O_i | \Psi \rangle = 0$ for any local operators O_i and O_j acting on qudits located at any nonadjacent vertices i and j . According to the expansion $O_i = \sum_{\alpha' \alpha} c_{\alpha' \alpha}^i |\alpha'\rangle \langle \alpha|$, $O_j = \sum_{\alpha' \alpha} c_{\alpha' \alpha}^j |\alpha'\rangle \langle \alpha|$, it suffices to show that $\langle \Psi | (\langle \bar{\alpha}' | \langle \bar{\alpha} |_j |\alpha'\rangle \langle \alpha|_i) | \Psi \rangle =$

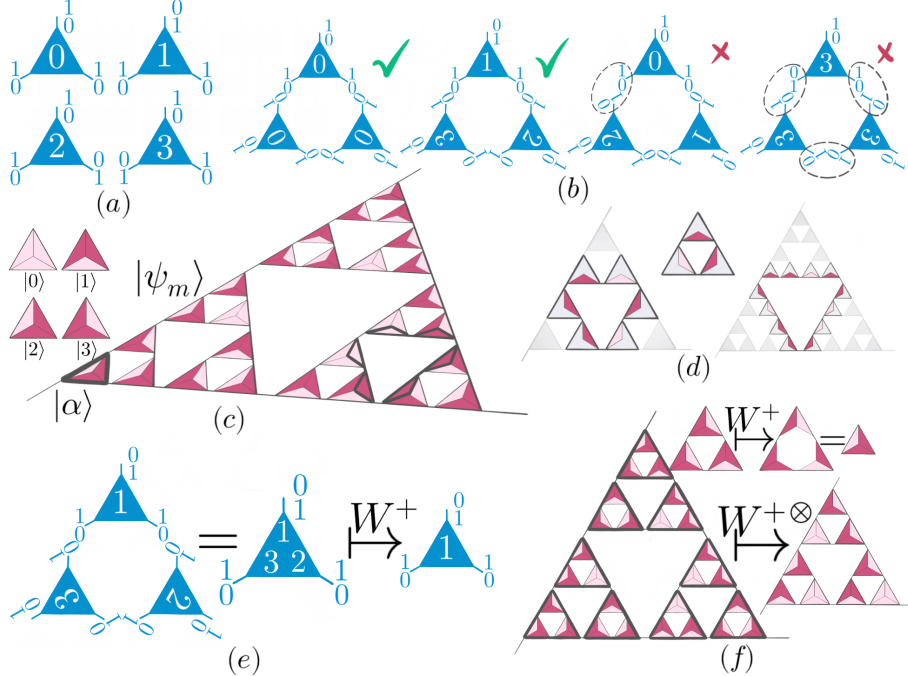


FIG. 5. (a) Tensors A_0, A_1, A_2 and A_3 which sum to A . (b) Example for nonvanishing (tick) and vanishing (cross) contraction of copies from A_0, A_1, A_2 and A_3 . (c) Illustration of $|\psi_m\rangle$ of the form $|\alpha\alpha'\alpha''\cdots\rangle$. $|\alpha\rangle$'s are represented by colored triangles with even number of red sides and odd number of pink sides. The orientation of the triangles is consistent with that of the tensors. (d) The circle structure in the Sierpiński lattice where the smallest circle is a block. Each vertex is simultaneously on three circles. The constraint on each circle that specifies $|\psi_m\rangle$ requires the number of red sides to be even. (e) Contraction of tensors A_1, A_2, A_3 which is eventually mapped to A_1 (up to a constant) through W^+ . (f) Illustration of the coarse graining and the self-similarity of $|\Psi\rangle$. The constraints specifying $|\psi_m\rangle$ are invariant to the coarse graining.

$\langle \Psi | (|\bar{\alpha}'\rangle\langle\bar{\alpha}|_j) | \Psi \rangle \langle \Psi | (|\alpha'\rangle\langle\alpha|_i) | \Psi \rangle = 0$ for any qudit basis states $|\alpha\rangle, |\alpha'\rangle, |\bar{\alpha}\rangle, |\bar{\alpha}'\rangle$.

We first consider the case where $|\alpha\rangle \neq |\alpha'\rangle$ (the case of $|\bar{\alpha}\rangle \neq |\bar{\alpha}'\rangle$ can be treated in a similar way). We observe that in the illustration of an arbitrary $|\psi_m\rangle$ (see Fig. 5(c), 5(d) and 6(a)), each triangle (a qudit basis state) is engaged in constraints on three circles (including the lateral sides) respectively as each triangle has three sides. It follows that the change from $|\alpha\rangle$ to $|\alpha'\rangle$ (as the color change on two sides of the triangle) on a vertex i will break the constraints on two circles (see Fig. 6(a)), resulting in a qudit-product-state $|\phi\rangle$ orthogonal to all the qudit-product-states expanding $|\Psi\rangle$. Then, if $|\bar{\alpha}\rangle = |\bar{\alpha}'\rangle$, we have $(|\bar{\alpha}\rangle\langle\bar{\alpha}|_j) |\psi_{m'}\rangle$ (either unchanged or equal to 0) is orthogonal to $|\phi\rangle = (|\alpha'\rangle\langle\alpha|_i) |\psi_m\rangle$ and hence both $\langle \Psi | (|\bar{\alpha}\rangle\langle\bar{\alpha}|_j) |\alpha'\rangle\langle\alpha|_i | \Psi \rangle$ and $\langle \Psi | (|\bar{\alpha}\rangle\langle\bar{\alpha}|_j) | \Psi \rangle \langle \Psi | (|\alpha'\rangle\langle\alpha|_i) | \Psi \rangle$ are zero. On the other hand, if $|\bar{\alpha}\rangle \neq |\bar{\alpha}'\rangle$, we also observe that the vertex j which is nonadjacent to i share at most one circle with i and the qudits on the two vertices respectively are at most commonly engaged in one constraint. Consequently, the change from $|\bar{\alpha}'\rangle$ to $|\bar{\alpha}\rangle$ on j maps $|\psi_{m'}\rangle$ to another qudit-product-state $|\phi'\rangle$ which is orthogonal to both $|\psi_m\rangle$ and $|\phi\rangle$ (as they differ by at least the constraint on one circle). Hence, both $\langle \Psi | (|\bar{\alpha}'\rangle\langle\bar{\alpha}|_j) |\alpha'\rangle\langle\alpha|_i | \Psi \rangle$ and $\langle \Psi | (|\bar{\alpha}'\rangle\langle\bar{\alpha}|_j) | \Psi \rangle \langle \Psi | (|\alpha'\rangle\langle\alpha|_i) | \Psi \rangle$ are zero, and we have the desired condition.

Then we consider the other case where $|\alpha\rangle = |\alpha'\rangle$ and $|\bar{\alpha}\rangle = |\bar{\alpha}'\rangle$. We firstly show that $\langle \Psi | (|\alpha\rangle\langle\alpha|_i) | \Psi \rangle = \langle \Psi | |\bar{\alpha}\rangle\langle\bar{\alpha}|_j | \Psi \rangle = 1/4$ for any basis state $|\alpha\rangle, |\bar{\alpha}\rangle$. To that end, we define local unitary operator $T_{ii'}$ for any pair of qudits on neighboring vertices i and i' as specified in Fig. 6(c). Note that $T_{ii'}$ has different forms for (i, i') in the same block and in two neighboring blocks [48], but the pictorial representation is the same as given by Fig. 6(c), thanks to our convention for representing the single-qudit-states by the triangles. Two important properties of $T_{ii'}$ acting on $|\psi_m\rangle$ can be directly read from Fig. 6(c): (1) $T_{ii'}$ preserves the constraints on all circles (including the lateral sides); (2) for a qudit on vertex i and in any $|\alpha\rangle$, the three unitary operators $T_{ii_1}, T_{ii_2}, T_{ii_3}$ (i_1, i_2, i_3 the three neighboring vertices of i) maps $|\alpha\rangle$ exactly to the other three basis states respectively (see Fig. 6(d)); (3) For cases where (i, i_2, i_3) forming a block while i_1 outside, $T_{ii_2}T_{ii_3}$ and T_{ii_1} map the single-qudit-state on i to the same state.

Now, as shown in Fig. 6(b), if in $|\psi_m\rangle$ the qudit on vertex i is in $|\alpha\rangle$, certain $T_{ii'}$ (or $T_{ii_2}T_{ii_3}$ for i at the corner) maps $|\psi_m\rangle$ exactly to a $|\psi_{m'}\rangle$ with the single-qudit-state on i changed from $|\alpha\rangle$ to $|\alpha'\rangle$. Since $T_{ii'}$ is unitary, it maps all $|\psi_m\rangle$'s with nonzero $\langle \psi_m | (|\alpha\rangle\langle\alpha|_i) | \psi_m \rangle$ one-to-one to all $|\psi_{m'}\rangle$'s with nonzero $\langle \psi_{m'} | (|\alpha'\rangle\langle\alpha'|_i) | \psi_{m'} \rangle$. Therefore, since $\sum_{\alpha=0}^3 \langle \Psi | (|\alpha\rangle\langle\alpha|_i) | \Psi \rangle = 1/M \sum_{\alpha=0}^3 \sum_m \langle \psi_m | (|\alpha\rangle\langle\alpha|_i) | \psi_m \rangle = 1$, we

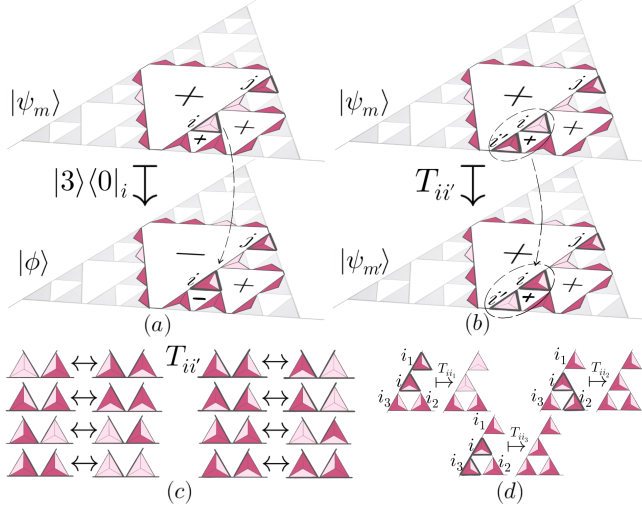


FIG. 6. (a) Operator $|3\rangle\langle 0|_i$ for the qudit on vertex i maps $|\psi_m\rangle$ to $|\phi\rangle$ which breaks the constraints on two circles. “+” for constraints satisfied on the corresponding circles and “-” for not satisfied. (b) Operator $T_{ii'}$ maps $|\psi_m\rangle$ to $|\psi_{m'}\rangle$, preserving the constraints on all circles. (c) The content of $T_{ii'}$ acting on a pair of neighboring qudits. (d) $T_{ii_1}, T_{ii_2}, T_{ii_3}$ acting on different neighboring pairs of qudits map the single-qudit-state $|1\rangle$ on vertex i to $|0\rangle$, $|3\rangle$ and $|2\rangle$ respectively.

have $\langle \Psi | (|\alpha\rangle\langle\alpha|_i) |\Psi\rangle = 1/4$ and similarly $\langle \Psi | |\bar{\alpha}\rangle\langle\bar{\alpha}|_j |\Psi\rangle = 1/4$. Next, we show $\langle \Psi | (|\bar{\alpha}\rangle\langle\bar{\alpha}|_j |\alpha\rangle\langle\alpha|_i) |\Psi\rangle = 1/16$. Indeed, following the spirit of the above arguments, we only need to notice that vertices i and j are nonadjacent so that $T_{ii'}$ leave the qudit on j unchanged (see Fig. 6(b)), and hence we have $\langle \Psi | (|\bar{\alpha}\rangle\langle\bar{\alpha}|_j |\alpha\rangle\langle\alpha|_i) |\Psi\rangle = \langle \Psi | (|\bar{\alpha}\rangle\langle\bar{\alpha}|_j |\alpha'\rangle\langle\alpha'|_i) |\Psi\rangle = 1/4 \times 1/4 = 1/16$. Obviously, it means that $\langle \Psi | (|\bar{\alpha}\rangle\langle\bar{\alpha}|_j |\alpha\rangle\langle\alpha|_i) |\Psi\rangle - \langle \Psi | (|\bar{\alpha}\rangle\langle\bar{\alpha}|_j) |\Psi\rangle \langle \Psi | (|\alpha\rangle\langle\alpha|_i) |\Psi\rangle = 1/16 - 1/16 = 0$. We have hence proved that $|\Psi\rangle$ has zero correlation length.

C. Proof for the system-size dependence of the circuit depth

Now, we consider arbitrary L and P and an arbitrary local quantum circuit U characterized by L and P . We prove that once the system is over certain size, U cannot completely disentangle $|\Psi\rangle$. To that end, we introduce another state $|\Phi\rangle$ which is orthogonal to $|\Psi\rangle$. Here $|\Phi\rangle = 1/\sqrt{M} \sum_m |\phi_m\rangle$ is the sum over all qudit-product-states satisfying constraints on all circles except for the largest four circles (see Fig. 7(a) and 7(b)). In the proof, we take advantage of the two-dimensional space spanned by $|\Psi\rangle$ and $|\Phi\rangle$ as a quantum code for detecting errors of the form U^+O_jU where O_j is a local operator located at some vertex j . Note that the space spanned by the orthonormal $|\Psi\rangle$ and $|\Phi\rangle$ detects an error, i.e. an operator O , if and only if $\langle \Psi | O | \Phi \rangle = \langle \Phi | O | \Psi \rangle = 0$ and $\langle \Psi | O | \Psi \rangle = \langle \Phi | O | \Phi \rangle$.

The proof is based on the following consideration. We assume that U completely disentangles $|\Psi\rangle$, i.e. $U|\Psi\rangle = \otimes_i |\chi_i\rangle$ with $|\chi_i\rangle$ being a normalized single-qudit-state on vertex i . Then, since $\langle U\Phi|U\Psi\rangle = \langle \Phi|U^+U|\Psi\rangle = \langle \Phi|\Psi\rangle = 0$, it is easy to show that there exists a local operator O_j located at some vertex j such that $\langle U\Psi|O_j|U\Psi\rangle \neq \langle U\Phi|O_j|U\Phi\rangle$. Indeed, expanding $|U\Phi\rangle$ in an arbitrary qudit-product-state basis including $\otimes_i |\chi_i\rangle$, qudit-product-states contributing to the expansion are orthogonal to $\otimes_i |\chi_i\rangle$, and hence there must be some $\otimes_i |\chi'_i\rangle$ with $\langle \chi'_j | \chi_j \rangle = 0$ at some vertex j . In that case, we can take O_j as $\mathbb{1} \otimes \cdots \otimes |\chi_j\rangle\langle\chi_j| \otimes \cdots \otimes \mathbb{1}$ so that we have $\langle U\Phi|O_j|U\Phi\rangle < 1$ and hence $\langle U\Phi|O_j|U\Phi\rangle \neq \langle U\Psi|O_j|U\Psi\rangle$. The inequality rewritten as $\langle \Phi|U^+O_jU|\Phi\rangle \neq \langle \Psi|U^+O_jU|\Psi\rangle$ implies that the space spanned by $|\Psi\rangle$ and $|\Phi\rangle$ does not detect the error U^+O_jU . According to this observation, we can prove that $|\Psi\rangle$ and $|\Phi\rangle$ detect all errors of the form U^+O_jU once the system is over certain size, which is more than enough to contradict the assumption, and hence to prove the desired result.

Following the above consideration, we now prove that once the linear size \mathcal{D} of the lattice is over $\frac{16}{3}PL - \frac{8}{3}P + \frac{5}{3}$ the error-detecting property is satisfied. In the graph-theoretical language, we define the linear size of the lattice (a connected subset) as the diameter of the lattice (subset) in the graph (induced subgraph) metric [49], consistent with the study of LRE in 2D [39]. Then, \mathcal{D} of a finite-generation Sierpiński lattice is exactly the number of links on one lateral side of the lattice as a triangle. There is another important size in our proof which is determined by the causal structure in the local quantum circuit (see the dark color in Fig. 7(c)): the operator $O_J = U^+O_JU$ is supported on a connected subset J of vertices with size $\mathcal{D}_J \leq (2L-1)P$ [50].

Now, we assume that the system is over certain size, i.e. the inequality $\mathcal{D} \geq \frac{16}{3}PL - \frac{8}{3}P + \frac{5}{3}$ or equivalently $\mathcal{D}_J \leq \frac{3}{8}\mathcal{D} - \frac{5}{8}$, and prove the error-detecting property.

We firstly prove $\langle \Psi | O_J | \Phi \rangle = \langle \Phi | O_J | \Psi \rangle = 0$. Indeed, it is easy to check that the distance between a closest pair of vertices respectively belonging to two separated circles among the four with broken constraints in $|\phi_m\rangle$ is $(\mathcal{D} - 1)/2$, greater than \mathcal{D}_J so that J can only cover vertices in one such circle. Consequently, $\langle \psi_{m'} | O_J | \phi_m \rangle = 0$ since O_J keeps $O_J |\phi_m\rangle$ with at least one constraint broken and different from that in $|\psi_{m'}\rangle$. Hence we have proved $\langle \Psi | O_J | \Phi \rangle = 0$, and $\langle \Phi | O_J | \Psi \rangle = 0$ as well using the same argument.

To prove $\langle \Psi | O_J | \Psi \rangle = \langle \Phi | O_J | \Phi \rangle$, we define unitary operators

$$\begin{aligned} S_i^1 &= |0\rangle\langle 1| + |1\rangle\langle 0| + |2\rangle\langle 3| + |3\rangle\langle 2|, \\ S_i^2 &= |0\rangle\langle 2| + |2\rangle\langle 0| + |1\rangle\langle 3| + |3\rangle\langle 1|, \\ S_i^3 &= |0\rangle\langle 3| + |3\rangle\langle 0| + |1\rangle\langle 2| + |2\rangle\langle 1|, \end{aligned}$$

acting on a single qudit located at the vertex i . As illustrated in Fig. 7(a) and 7(d), the effect of these operators is to exchange the red and pink on two sides of the tri-

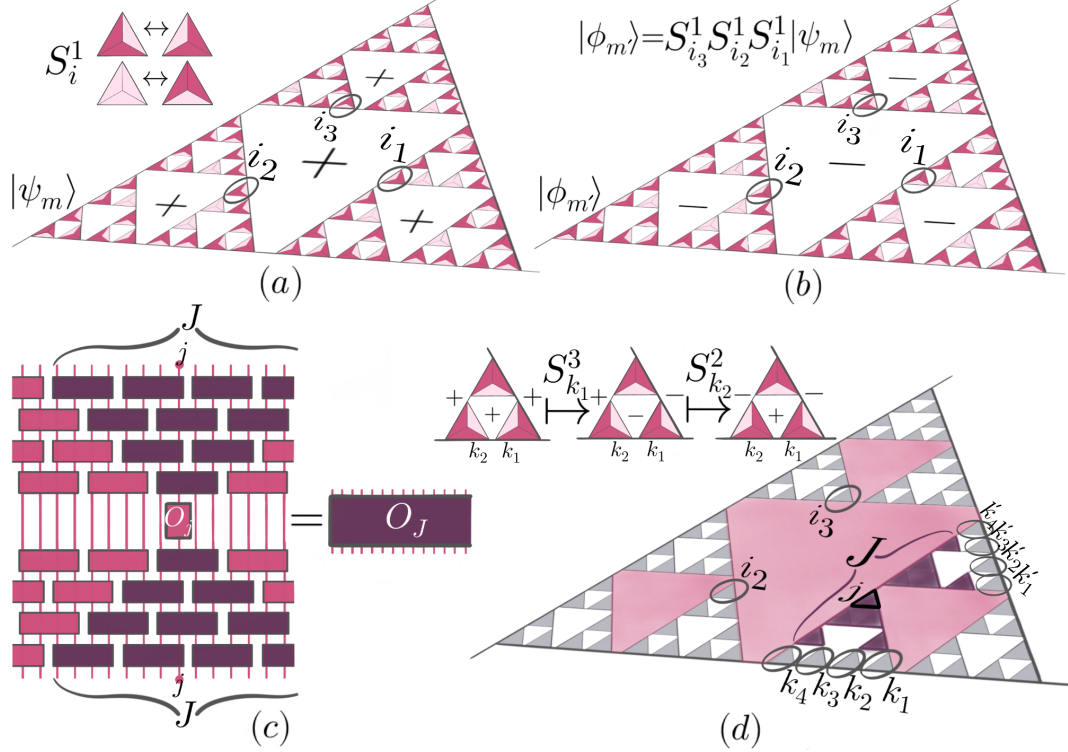


FIG. 7. (a) The qudit-product state $|\psi_m\rangle$ which satisfies all constraints and the illustration of the unitary operator S_i^1 . (b) The qudit-product state $|\phi_{m'}\rangle$ which satisfies all constraints except for the four on the largest four circles. “+” for constraints satisfied on the corresponding circles and “-” for not satisfied. The unitary operator $V_1 = S_{i_3}^1 S_{i_2}^1 S_{i_1}^1$ maps $|\psi_m\rangle$ to $|\phi_{m'}\rangle$. (c) The causal structure in the local quantum circuit which extends the support of O_j as a single vertex to the support J of O_j as a connected subset of vertices. (d) The size of support J which does not overlap with the path $K = \{k_1, k_2, k_3, k_4\}$ or $K' = \{k'_1, k'_2, k'_3, k'_4\}$ linking two neighboring largest circles. The unitary operator $V_2 = S_{i_3}^1 S_{i_2}^1 S_{k_4}^2 S_{k_3}^3 S_{k_2}^2 S_{k_1}^3$ or $V_3 = S_{i_3}^1 S_{i_2}^1 S_{k'_4}^3 S_{k'_3}^2 S_{k'_2}^3 S_{k'_1}^2$ maps $|\psi_m\rangle$ to $|\phi_{m'}\rangle$.

angle or create two red (pink) sides from two pink (red) sides. Then, since vertex i is simultaneously included in three circles (including the lateral sides), applying S_i^1, S_i^2 or S_i^3 to $|\psi_m\rangle$ simply breaks the constraints on two out of the three circles according to the superscript 1, 2, 3. With these unitary operators, we can define a unitary operator $V_1 = S_{i_3}^1 S_{i_2}^1 S_{i_1}^1$ where each of the three vertices i_1, i_2, i_3 is included in two out of the four largest circles. As shown in Fig. 7(a) and 7(b), V_1 simply break the constraints on the four circles and maps $|\psi_m\rangle$ to $|\phi_{m'}\rangle$ and hence maps $|\Psi\rangle$ to $|\Phi\rangle$.

Now, there are two cases to be considered regarding the support J of O_j : (1) J does not cover any of i_1, i_2, i_3 ; (2) J covers only one of the three vertices. Indeed, as we have shown, J cannot cover more than one of the three vertices since they are farther apart beyond the size \mathcal{D}_J . In case (1), we have $[O_j, V_1] = [O_j, V_1^+] = 0$. It follows that $\langle \Phi | O_j | \Phi \rangle = \langle V_1 \Psi | O_j | V_1 \Psi \rangle = \langle \Psi | V_1^+ O_j V_1 | \Psi \rangle = \langle \Psi | V_1^+ V_1 O_j | \Psi \rangle = \langle \Psi | O_j | \Psi \rangle$ as desired. In case (2), without loss of generality, we suppose the covered vertex

is i_1 . Then we can define another two unitary operators

$$V_2 = S_{i_3}^1 S_{i_2}^1 S_{k_{(\mathcal{D}+1)/4}}^2 \cdots S_{k_2}^2 S_{k_1}^3,$$

$$V_3 = S_{i_3}^1 S_{i_2}^1 S_{k'_{(\mathcal{D}+1)/4}}^3 \cdots S_{k'_2}^3 S_{k'_1}^2,$$

where the two subsets of vertices $K = \{k_1, k_2, \dots, k_{(\mathcal{D}+1)/4}\}$ and $K' = \{k'_1, k'_2, \dots, k'_{(\mathcal{D}+1)/4}\}$, as specified in Fig. 7(d) form the two paths connecting two adjacent largest circles. Note that any $k \in K$ and $k' \in K'$ have distance $(\mathcal{D}+1)/4, (\mathcal{D}+1)/4 - 1$ to i_1 respectively. Then, since i_1 is covered in J , J cannot have overlap with both K and K' , otherwise the distance between the k and k' (in the overlap) within J exceeds the size \mathcal{D}_J , which implies contradiction. Indeed, due to the inequality $\mathcal{D}_J \leq \frac{3}{8}\mathcal{D} - \frac{5}{8}$, J cannot cover the whole of or encircle any of the four circles, since any connected region encircling such a circles has size at least equal to $\frac{3}{8}\mathcal{D} + \frac{3}{8} > \mathcal{D}_J$. Hence, if k and k' are both in J , the shortest path connecting them (which defines their distance with J) must pass through i_1 , giving rise to the distance $\frac{1}{2}\mathcal{D} - \frac{1}{2} > \mathcal{D}_J$. Consequently, we have either $[O_j, V_2] = [O_j, V_2^+] = 0$ or $[O_j, V_3] = [O_j, V_3^+] = 0$, which leads to $\langle \Psi | O_j | \Psi \rangle = \langle \Phi | O_j | \Phi \rangle$ by the same

arguments as in case (1).

Above arguments have proved the error-detecting property, and that any U characterized by given P and L cannot completely disentangle $|\Psi\rangle$ once the system size is large enough. Together with the zero correlation length proved in the previous subsection, we have proved the LRE in $|\Psi\rangle$. We have also proved that for given P , the depth L for any local quantum circuit characterized by P and L to completely disentangle $|\Psi\rangle$ has a lower bound $L > \frac{3}{16P}\mathcal{D} + \frac{1}{2} - \frac{5}{16P}$ which is linear to the lattice linear size \mathcal{D} .

D. A new paradigm of LRE

Now, we compare the LRE pattern in $|\Psi\rangle$ and the SRE pattern in the previous example as characterized by their distinct constraints shown pictorially in Fig. 5(c) and 3(b) respectively. Based on the perspective that quantum orders are essentially distinct entanglement patterns, we try to reveal the novelty in the LRE pattern.

While the SRE pattern exhibits how minimal or shortest-range information encoded in qudits is compatible with the fractal self-similarity, the LRE pattern exhibits how nonlocally encoded information survives in the fractal zoom-in and zoom-out operations. Here, without resorting to technical treatment, we can understand the encoded nonlocal information as the very property of $|\Psi\rangle$ which prevents constant-depth local quantum circuit from disentangling the state.

Intriguingly, such nonlocal information encoded in $|\Psi\rangle$ is not formed by long-range correlation of qudits, but on the contrary “dissolves” the correlation length so that any distant pair of qudits are not correlated. This paradoxical property (the essence of LRE) portrays a highly nontrivial ordering of qudits in fractal geometry. In the following, we will show that such ordering reveals the existence of a new paradigm for realizing LRE in addition to the picture of topological order.

Note that based on the tensor-network representation of $|\Psi\rangle$, there are different local Hamiltonians which can stabilize $|\Psi\rangle$ as a ground state. Instead of going into a specific Hamiltonian, here, we focus on the manner that nonlocal information is encoded in $|\Psi\rangle$.

As we have pointed out, the concepts of bulk and boundary cannot be defined on the Sierpiński lattice. It follows that the underlying objects of topological order, i.e. the topology of manifold is incompatible with our system. Indeed, a recent work [24] shows that 2D topological order cannot be adjusted to fractal lattice systems with dimension between 1D and 2D, and has hence formally negated that $|\Psi\rangle$ is realized within an (extended) paradigm of topological order. Here, we apply the general idea of Ref. [24] to our case, and explicitly show the fundamental difference between the manner that the nonlocal information is encoded in topologically ordered states and the manner in our case.

To compare $|\Psi\rangle$ with topologically ordered states in a

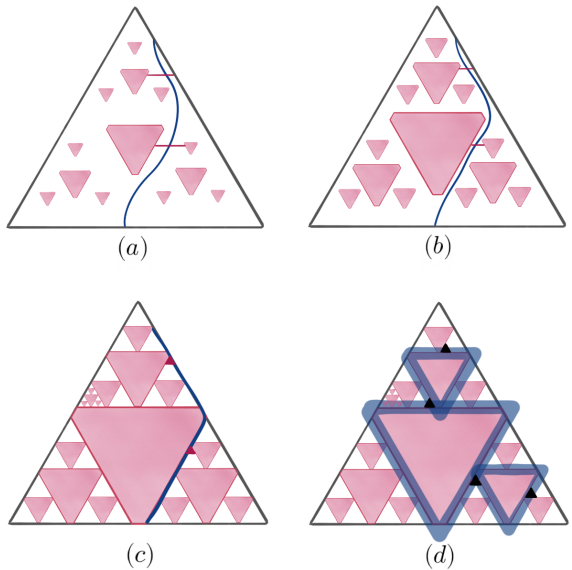


FIG. 8. (a) and (b) illustrate regular lattices with holes (the pink regions) where the white region represents vertices in a regular geometry. There can be open or closed boundaries. For simplicity in the illustration, we do not distinguish them. The blue line represents a macroscopic logical string operator while the red line represents logical string operators of different type that links the boundaries of two holes. The two ends of such lines should be understood as on the same type of boundary. Keeping enlarge the size of holes, (a) and (b) converge to (c) where the red line is squeezed into a vertex (the red dot). Keeping punch holes from (c) results in a finite-generation Sierpiński lattice. The bold blue lines in (d) illustrate how qudits (the black dots) are entangled in $|\Psi\rangle$ through the interlocking circles.

comparable setting, we consider a sequence of lattices as illustrated in Fig. 8(a) and 8(b) where a number of holes (the pink regions) are punched from a regular lattice. In these lattices, the bulk (the white region) is formed by the vertices between the boundary of these holes and the lateral sides of the triangle. This way, the picture of topological order can be defined with allowable modification, i.e. with closed or open gapped boundaries of these holes and the lateral sides which condensate anyons (see the formal treatment in Ref. [24, 51]). The sequence of lattices converges to a lattice illustrated by Fig. 8(c) from which keeping punching holes eventually results in a finite-generation Sierpiński lattice. Note that the circles in the Sierpiński lattice can be viewed as originating from the boundary of those holes in Fig. 8(a) and 8(b).

As an example, the 2D \mathbb{Z}_N topological order on lattices as Fig. 8(a) and 8(b) is characterized by the code distance which increases along the increasing system size and plays the role corresponding to our notation \mathcal{D}_J (see Sec. VI C) in giving rise to LRE, i.e. in the quantum-error-detecting property [39]. The nonlocal information is encoded in entangled local degrees of freedom as logical qubits, and only representative of (homologically nontrivial) string operators (the blue or the red lines in Fig. 8(a)

and 8(b)) that can be deformed into each other through the bulk region can operate on. In this sense, the non-local information can be understood as spreading over the bulk region. An important fact is that the shortest strings (red) and the longest strings (blue) of different types intersect for odd times and hence do not commute so that nonlocal information encoded is confined by the shortest string operators, i.e. the code distance. Consequently, in converging to Fig. 8(c), the code distance in Fig. 8(a) and 8(b) is being squeezed, approaching the size of a single vertex, independent on the system size, i.e., the topological order is disappearing. Furthermore, the bulk region is being squeezed into isolated local regions (connected only through single vertices) so that the nonlocality of the encoded information is being undermined. In other words, the self-similar pattern of holes in Fig. 8(c) excludes the paradigm of topological order and the correspondingly realized LRE in ground states.

However on the contrary, the LRE in $|\Psi\rangle$ is exactly realized through the self-similar pattern of circles in Fig. 8(d), as originated from the boundaries of the holes in Fig. 8(c). Indeed, as shown in the proof in Sec. VI C, constant-depth local quantum circuit cannot completely disentangle $|\Psi\rangle$ simply because the circuit cannot disentangle the circles once the system size is large enough. In other words, as illustrated in Fig. 8(d), the nonlocal information in $|\Psi\rangle$ is simply encoded through the interlocking circles which correlates all local degrees of freedom through the self-similar pattern. To sum up, the nonlocal information in $|\Psi\rangle$ and in topologically ordered state are encoded with the help of essentially different geometries intrinsic to the different spatial dimensions: While the self-similar patterns of circles squeeze the bulk out and hence exclude topological order, they exactly give rise to the LRE in $|\Psi\rangle$.

The above arguments have clearly revealed the existence of a new paradigm for realizing LRE patterns in addition to the topological picture. Since topological order has been the only known paradigm for realizing LRE in 2D, our example indeed evidences a novel quantum order inherent to the fractal geometry and the fractional spatial dimension. A comprehensive characterization of such novel ordering requires systematic study on how the LRE reveals itself in excitation properties of certain Hamiltonians which stabilize $|\Psi\rangle$ as a ground state. This will be included in a separated work of the author since it is beyond the scope of the present work which focuses on entanglement patterns. Indeed, the coexistence between the short-range correlation and the nonlocally encoded information in $|\Psi\rangle$ implies a formula of entanglement entropy analogous to the topological entanglement entropy in 2D [35, 36], i.e. with universal terms of different meaning from topology. This will also be included in a separated work of the author.

E. Toy model of multi-layer hardcore bosons

We end the discussion on the LRE pattern with a toy model of strongly interacting hardcore bosons whose unique ground state simulates $|\Psi\rangle$. Similar to Sec. V, we choose the model of hardcore bosons for its realizability in different experimental settings and its high controllability in both spatial geometry and forms of boson-boson coupling [44, 45]. Among different models which can stabilize $|\Psi\rangle$ as a ground state, we expect that the model we introduce here might shed light on finding experimentally realizable models for realizing the LRE patterns of quantum states in fractional dimension. Note that recent work on realizing 2D LRE states through quantum circuit without resorting to a specific Hamiltonian [31] also demonstrates another direction towards the application of LRE in quantum computation.

We follow the discussion of the toy model introduced in Sec. V and consider a multilayer structure. As shown in Fig. 9(a), each layer is not a complete Sierpiński lattice, but a sublattice as 1D rings or chains of the same size corresponding to the circles and the lateral sides of the Sierpiński lattice. This way, all layers can be superimposed to give the Sierpiński lattice structure where each vertex i of the superimposed Sierpiński lattice only appears in three layers (see Fig. 9(a)) since each vertex of the Sierpiński lattice is included in three circles (or lateral sides). As we will show, the occupations of hardcore bosons on the same vertex but in the different three layers can be coupled into the \mathbb{C}^4 qudit degrees of freedom (see Fig. 9(b)).

The Hamiltonian is defined as

$$H = -t \sum_r \sum_{(k,l) \in r} a_k^r + a_l^r + a_k^r + a_l^r + \text{c.c.} + v \sum_i (n_i^s - 1/2)(n_i^{s'} - 1/2)(n_i^{s''} - 1/2). \quad (4)$$

Here, the quantum fluctuation with amplitude t is generated by the hopping and the creation (annihilation) of pairs of bosons on nearest neighboring vertices of each ring (chain) r in each layer s (see Fig. 9(a)). The layers are coupled through an interlayer interaction with strength v in the z -direction on each individual vertex i of the superimposed Sierpiński lattice. Each interaction term include the bosons on the three layers s , s' and s'' where the vertex i appears (see Fig. 9(a)). Note that H creates or annihilates bosons in pairs so that the parity of particle numbers on each ring (chain) is preserved. Here, we choose to work in the sector in which each ring (chain) accommodates even number of bosons.

We solve the model in the strong-interaction limit $t \ll v$ using the same perturbation method as discussed in Sec. V. In specifying the Hilbert space \mathcal{H}_0 of states with lowest interaction energy, we notice that each interaction term $v(n_i^s - 1/2)(n_i^{s'} - 1/2)(n_i^{s''} - 1/2)$ favors Fock states with either no bosons occupying the vertex i in any layer or with two hardcore bosons occupying

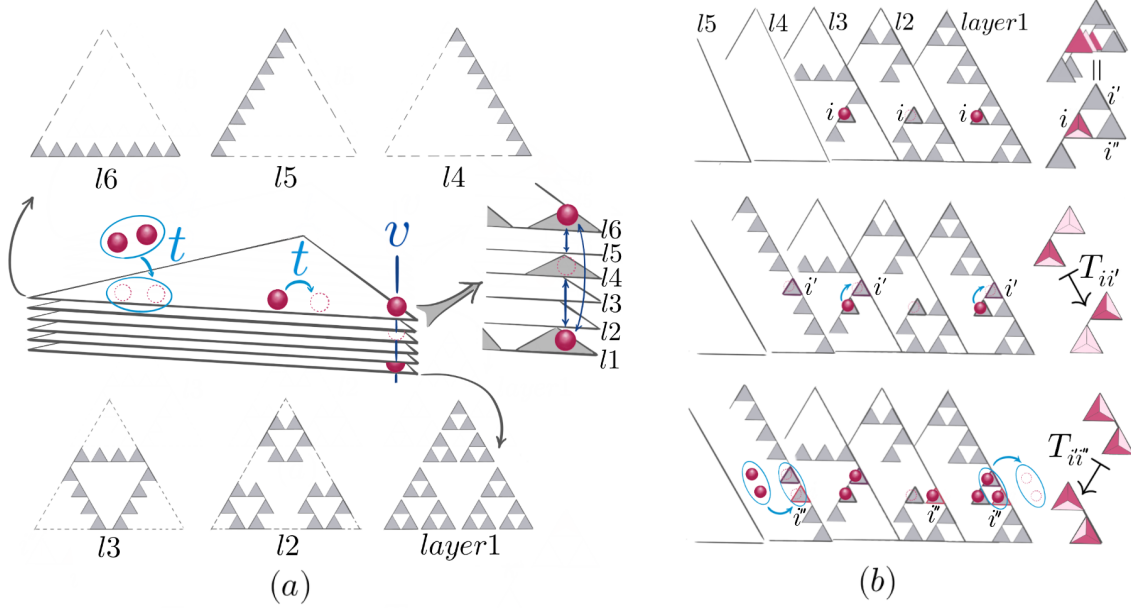


FIG. 9. (a) The model of multilayer hardcore bosons. Each layer is a sublattice of the Sierpiński lattice, i.e. 1D rings or 1D chains of the same size. Each vertex of the Sierpiński lattice is included in exactly three layers here as each vertex is included in three circles (lateral sides) in the Sierpiński lattice. Note that layer 1 is isolated 1D rings formed by the blocks. Within each ring or chain, there are hopping and creation (annihilation) of pairs of bosons. The interlayer interaction on each vertex engages bosons on the three layers including the vertex. (b) The upper shows how occupation numbers on the three layers 1, 2 and 3 including the vertex i is mapped to a qudit state $|\alpha\rangle$. The middle and the lower show how the second order perturbation terms $a_i^3 + a_i^3 a_{i'}^1 + a_i^1$ and $a_{i'}^4 + a_{i''}^4 + a_i^1 a_{i''}^1$ act on the effective qudit states as the effect of the $T_{ii'}$ and $T_{ii''}$ operators.

the vertex i on two different layers, i.e., with eigenvalue $-v/8$ (the other eigenvalue is $v/8$). It follows that in such Fock states, the occupation numbers $(x_s, x_{s'}, x_{s''}) = (0, 0, 0), (0, 1, 1), (1, 0, 1), (1, 1, 0)$ can be identified with the qudit basis states $|\alpha\rangle = |0\rangle, |1\rangle, |2\rangle, |3\rangle \in \mathbb{C}^4$ so that such Fock states have the effective form $|\alpha, \alpha', \alpha'', \dots\rangle$ as a qudit-product state.

We can further represent $(x_s, x_{s'}, x_{s''})$ by a colored triangle as we used in Fig. 5(c) (occupation number 1 for red side and 0 for pink side) with certain convention. We illustrate such convention in Fig. 9(b) (upper) where we have $s = l1, s' = l2, s'' = l3$, and $x_s = 1, x_{s'} = 0, x_{s''} = 1$ correspond to the occupation on the three different circles or lateral sides (1D rings or chains) including the vertex i . We set the orientation of the triangle such that the side representing x_s is towards the circle on the layer $s = l1$ and others in the same way. This convention is further illustrated at vertices i', i'' in Fig. 9(b) (middle and lower). Then, compared with Fig. 5(d), the red sides of the triangle is on the circles where bosons are occupied at vertex i . Since each 1D ring or chain has even occupation of bosons, the number of red sides on each circle is even, consistent with the description in Fig. 5(c) and 5(d). In other words, Fock states with the lowest interaction energy and of the form $|\alpha, \alpha', \alpha'', \dots\rangle$ can be identified with the $|\psi_m\rangle$'s spanning $|\Psi\rangle$. Consequently, the representation of $(x_s, x_{s'}, x_{s''})$'s with the colored triangles maps \mathcal{H}_0 unitarily to the subspace of $(\mathbb{C}^4)^\otimes$ spanned by the $|\psi_m\rangle$'s.

In specifying H_{eff} within \mathcal{H}_0 and its equivalent form for qudits, we notice that the lowest-order nonvanishing perturbation terms preserving the interlayer interaction energy has one of the eight forms

$$\begin{aligned} & a_k^{r+} a_l^r a_k^{r'+} a_l^r, \quad a_k^{r+} a_l^r a_l^{r'+} a_k^r, \\ & a_k^{r+} a_l^r a_k^{r'+} a_l^{r'+}, \quad a_k^{r+} a_l^r a_k^{r'} a_l^r, \\ & a_k^{r+} a_l^r a_k^{r'+} a_l^{r'+}, \quad a_k^{r+} a_l^r a_k^{r'} a_l^r, \\ & a_k^{r+} a_l^r a_k^{r'+} a_l^r, \quad a_k^r a_l^r a_k^{r'+} a_l^r, \end{aligned}$$

or their eight complex conjugate forms. Here r and r' are two 1D rings (lateral sides) in two different layers both including the nearest neighboring vertices k and l . Note that here we omit the terms of the form $a_k^{r+} a_l^r a_l^{r'+} a_k^r$ and $a_k^{r+} a_l^r a_k^{r'} a_l^r$ (or their conjugates), since these terms together give a constant operator, which do not contribute to solving H_{eff} . Indeed, as illustrated in Fig. 9(b) (middle and lower), it can be easily shown that the sum of all these terms for $r \neq r'$ on the vertices k and l , as mapped to the subspace of qudits, have exactly the forms of T_{kl} as introduced in Sec. VI B and defined in Fig. 6(c). Consequently, according to the perturbation method as discussed in Sec. V, H_{eff} has the form in the equivalent qudit space

$$H_{\text{eff}} = -2t^2/v \sum_{kl} T_{kl}, \quad (5)$$

where $v/2$ is the interaction energy difference and the minus sign originates from the unperturbed Green function.

To solve the ground state of H_{eff} , we take advantage of the fact that all T_{kl} terms commute with each other, as can be easily shown with its definition in Fig. 6(c). Furthermore each T_{kl} has the spectra $(-1, 1)$ with projection operator $(1 - T_{kl})/2$ and $(1 + T_{kl})/2$ respectively, since it is self-adjoint and also unitary. Hence, H_{eff} describes a gapped system with the ground state subspace $\prod_{kl} \frac{(1+T_{kl})}{2} \mathcal{H}_0$. Obviously, $|\Psi\rangle = 1/\sqrt{M} \sum_m |\psi_m\rangle$ is a ground state since $T_{kl} |\Psi\rangle = |\Psi\rangle$ for all (k, l) . To show that $|\Psi\rangle$ is the unique ground state, we need to prove that T_{kl} 's are ergodic in \mathcal{H}_0 , i.e. for any $|\psi_m\rangle$ and $|\psi_{m'}\rangle$, we have $|\psi_{m'}\rangle = T_{k' l'} \cdots T_{kl} |\psi_m\rangle$. The detail of the proof is given in App. B, and the basic idea is to prove that any $|\psi_m\rangle$ can be mapped to $|\psi_{m_0}\rangle = |000\cdots\rangle$ by applying the T_{kl} terms on a finite number of neighboring qudits. Note that here $|0\rangle$ is the basis state of the qudit, not the occupation number. Then, according to the Perron-Frobenius theorem [52], ergodicity of T_{kl} 's in H_{eff} implies the uniqueness of the ground state $|\Psi\rangle$. Therefore, we can conclude that the model H of strongly interacting hardcore bosons effectively simulates $|\Psi\rangle$ as the unique ground state.

VII. CONCLUSION

We have provided a concrete example of long-range entanglement (LRE) in fractional spatial dimension, i.e. a state with zero correlation length but cannot be completely disentangled by constant-depth local quantum circuits. The LRE in our example results from the compatibility between fractal self-similarity and nonlocal information encoded in entangled local degrees of freedom, instead of resulting from topology. It reveals a new paradigm for realizing LRE patterns in addition to the picture of topological order. Furthermore, following the perspective that quantum orders are portrayed by distinct entanglement patterns, our example evidences a novel quantum order inherent in quantum matters of fractional spatial dimension.

It is worth noting that our example is simply generated from a single tensor satisfying certain scale-invariance equation and with the lowest nontrivial bond dimension. It implies the existence of a large playground of nontrivial entangled states in fractal geometry and in fractional dimension as the microscopic origins of novel quantum phase of matter. Our framework for studying entanglement-renormalization fixed points in terms of tensor networks also establishes the equivalence between scale invariance and self-similarity in entanglement, and can be applied to a wide classes of fractal lattice geometries.

More importantly, our results unveil the novelty and the distinctiveness in studying quantum phases and states of fractal quantum matter or quantum matter in fractional spatial dimension. These results are also ex-

pected to initiate new study on emergent properties of quantum many-body systems. Indeed, there are many inspiring open questions. For example, the seemingly contradictory numerical evidences of anyons [15] in fractal geometry and theoretical negation of topological order [24] in fractional dimensions between 1D and 2D call for new understanding of quantum order in fractional dimension.

Lastly, our work has raised the question: Will LRE patterns in fractional dimension, e.g., the one given in our work, play similar roles as the 2D LRE states in the application to quantum information science? This question will be partially answered in a separate work of the author. As what we have shown and what we will show, quantum order and entanglement in fractal geometries, or more generally, fractional dimensions, provide a new direction for discovering the deep connection between quantum matter and quantum information.

VIII. ACKNOWLEDGEMENTS

The author thanks Anne E. B. Nielsen for inspiring discussions on the tensor-network description of scale invariance and self-similarity. The author thanks Wei Ku, Jinwu Ye and Jianda Wu for fruitful discussions on quantum order and quantum correlations. These discussions partially motivated this work. The author also thanks Haiyuan Zou and Fangyuan Gu for useful comments on the manuscript. This work is supported by the Tsung-Dao Lee Institute Postdoctoral Fellowship Grant.

Appendix A: Self-similar tensor network

In this section, we prove the equivalence between the following two equations describing the scale invariance of a fixed point as contracted from copies of the tensor $A \in \mathbb{C}^d \otimes \mathbb{C}^{D^3}$,

$$W^+ \text{Tr}_{\{\mathbb{C}^D\}}[A \otimes A \otimes A] = \lambda A, \quad (\text{A.1})$$

$$\text{Tr}_{\{\mathbb{C}^{2D}\}}[\mathbf{E} \otimes \mathbf{E} \otimes \mathbf{E}] = |\lambda|^2 \mathbf{E}. \quad (\text{A.2})$$

We present our proof in a general framework where the number of virtual indices is not important so that our results can be easily applied to a wide class of fractal geometries. The only requirement is that the contraction of a block of tensors keeps the lattice geometry which reflects the self-similarity.

Through our proof, we view A as a linear map $A : \mathbb{C}^{D^3} \rightarrow \mathbb{C}^d$, and $A^+ : \mathbb{C}^d \rightarrow \mathbb{C}^{D^3}$, $\mathbf{E} = A^+ A : \mathbb{C}^{D^3} \rightarrow \mathbb{C}^{D^3}$ as well. This treatment takes advantage of the isomorphism $|\alpha\beta\beta'\beta''\rangle \mapsto |\alpha\rangle\langle\beta\beta'\beta''|$ between the space $\mathbb{C}^d \otimes \mathbb{C}^{d^3}$ and the operator space $\mathbf{L}(\mathbb{C}^{d^3}, \mathbb{C}^d)$. This way, many important properties of tensor network can be easily shown without considering the specifics

of virtual indices. Note that the contraction of tensors or the trace operation can also be viewed as composition of linear maps. For example, the contractions $\mathbf{A} = \text{Tr}_{\{\mathbb{C}^D\}}[A \otimes A \otimes A]$ and $\mathbf{A}^+ = \text{Tr}_{\{\mathbb{C}^D\}}[A^+ \otimes A^+ \otimes A^+]$ as illustrated in Fig. 1(e) and Fig. 2(a) can be represented as the composition

$$\begin{aligned} \mathbb{C}^{D^3} &\xrightarrow{\text{Tr}_{\{\mathbb{C}^D\}}^+} (\mathbb{C}^{D^3})^{\otimes 3} \xrightarrow{A^{\otimes 3}} (\mathbb{C}^d)^{\otimes 3} \\ &(\mathbb{C}^d)^{\otimes 3} \xrightarrow{(A^+)^{\otimes 3}} (\mathbb{C}^{D^3})^{\otimes 3} \xrightarrow{\text{Tr}_{\{\mathbb{C}^D\}}} \mathbb{C}^{D^3}, \end{aligned}$$

giving $\mathbf{A} : \mathbb{C}^{D^3} \rightarrow (\mathbb{C}^d)^{\otimes 3}$ and $\mathbf{A}^+ : (\mathbb{C}^d)^{\otimes 3} \rightarrow \mathbb{C}^{D^3}$ respectively, where we have

$$\begin{aligned} \text{Tr}_{\{\mathbb{C}^D\}} &= \sum_{\beta\beta'\beta''} \sum_{\beta_1\beta'_1\beta''_1} |\beta\beta'\beta''\rangle\langle\beta\beta_1\beta''_1\beta'\beta'_1\beta_1\beta''\beta''_1\beta'_1| \\ \text{Tr}_{\{\mathbb{C}^D\}}^+ &= \sum_{\beta\beta'\beta''} \sum_{\beta_1\beta'_1\beta''_1} |\beta\beta_1\beta''_1\beta'\beta'_1\beta_1\beta''\beta''_1\beta'_1\rangle\langle\beta\beta'\beta''|. \end{aligned}$$

We can write the linear-map form of Eq. A.1 simply as $W^+ \mathbf{A} = \lambda A$.

1. From Eq. A.1 to Eq. A.2

We assume Eq. A.1. To prove Eq. A.2, we take advantage of the basic property of tensor contraction, i.e., in contracting the three copies of \mathbf{E} , we can firstly contract the three copies of A and the three copies of A^+ on their virtual indices respectively and then contract \mathbf{A} and \mathbf{A}^+ on their physical indices (see Fig. A.1). In other words, we have $\text{Tr}_{\{\mathbb{C}^{2D}\}}[\mathbf{E} \otimes \mathbf{E} \otimes \mathbf{E}] = \mathbf{A}^+ \mathbf{A}$. Then, we note that the coarse graining operator W^+ exactly extracts the degrees of freedom in charge of the entanglement between each block and its neighboring blocks. In the linear-map formalism, it means that the image of the isometry W equals the image of the contracted \mathbf{A} , i.e. the degrees of freedom correlated with the remaining virtual indices after the contraction $\mathbf{A} = \text{Tr}_{\{\mathbb{C}^D\}}[A \otimes A \otimes A]$ (those connecting one block with its neighbors). It follows that WW^+ equals the projection on $\text{Im}\mathbf{A} = \text{Im}W$, which, combined with Eq. A.1, gives $WW^+ \mathbf{A} = \mathbf{A} = \lambda WA$. We can illustrate the new equation and its adjoints in a diagram of linear maps

$$\begin{array}{ccccc} \mathbb{C}^{D^3} & \xrightarrow{A} & (\mathbb{C}^d)^{\otimes 3} & \xrightarrow{A^+} & \mathbb{C}^{D^3} \\ \lambda A \downarrow & \nearrow W & & \searrow W^+ & \uparrow \lambda^* A^+ \\ \mathbb{C}^d & & & & \mathbb{C}^d \end{array} \quad . \quad (\text{A.3})$$

Obviously, this diagram is commutative in the sense that the compositions of maps guided by the arrows from any given space to another given space are all equal. Then, since W^+W is the identity map, we have $\lambda^* \lambda A^+ W^+ W A = \lambda^* \lambda A^+ A = |\lambda|^2 \mathbf{E} = \mathbf{A}^+ \mathbf{A} = \text{Tr}_{\{\mathbb{C}^{2D}\}}[\mathbf{E} \otimes \mathbf{E} \otimes \mathbf{E}]$ as desired.

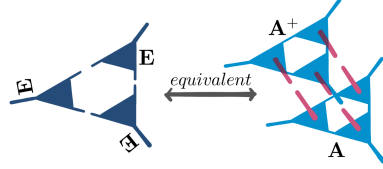


FIG. A.1. The equivalence between two contraction schemes.

2. From Eq. A.2 to Eq. A.1

Now we assume Eq. A.2 and also assume that we don't know the existence of A and the space \mathbb{C}^d either, but only have \mathbf{E} as a positive operator belonging to $\mathbf{L}(\mathbb{C}^{D^3})$. This way we start with the minimal conditions on \mathbf{E} . Note that every transfer matrix is automatically a positive operator in the linear-map formalism by definition.

We firstly define A with the desired property from a given positive operator \mathbf{E} . To that end, we consider the quotient space $\mathbb{C}^{D^3}/\text{Ker}\mathbf{E}$ together with the surjective quotient map $\pi : \mathbb{C}^{D^3} \rightarrow \mathbb{C}^{D^3}/\text{Ker}\mathbf{E}$ and the injective map $g : \mathbb{C}^{D^3}/\text{Ker}\mathbf{E} \rightarrow \mathbb{C}^{D^3}$ satisfying $g\pi = \mathbf{E}$. Here, π will be the desired A , but we still have to define the inner product on the quotient space in order to make it a Hilbert space and define the adjoint of A . We define the inner product by $\langle \pi\beta | \pi\beta' \rangle = \langle \beta | \mathbf{E} \beta' \rangle$. It is easy to check that the inner product is well-defined. Then, π^+ can be defined and we have $\langle \beta | \pi^+ \pi \beta' \rangle = \langle \pi\beta | \pi\beta' \rangle = \langle \beta | \mathbf{E} \beta' \rangle = \langle \beta | g\pi \beta' \rangle$, which means that $g\pi = \pi^+ \pi$, and hence $g = \pi^+$ since π is surjective. Consequently, defining $A = \pi$, we have $A^+ A = \pi^+ \pi = g\pi = \mathbf{E}$. If we further choose the right physical dimension d to identify the Hilbert space $\mathbb{C}^{D^3}/\text{Ker}\mathbf{E}$ with \mathbb{C}^d , we recover the linear map (tensor) A in Eq. A.1.

Next, we derive Eq. A.1 from a basic algebraic property of A as the quotient map. We consider an arbitrary $A' : \mathbb{C}^{D^3} \rightarrow \mathbb{C}^{d'}$ also satisfying $A'^+ A' = \mathbf{E}$. It can be easily proved that $\text{Ker}A' = \text{Ker}\mathbf{E}$ according to $\langle \beta | A'^+ A' \beta' \rangle = \langle A' \beta | A' \beta' \rangle$. Because of that, we have a well-defined linear map $V : \mathbb{C}^d \rightarrow \mathbb{C}^{d'}$ by $|A\beta\rangle \mapsto |A'\beta\rangle$ which is an isometry since $\langle A\beta | A\beta' \rangle = \langle \beta | A^+ A \beta' \rangle = \langle \beta | \mathbf{E} \beta' \rangle = \langle \beta | A'^+ A' \beta' \rangle = \langle A' \beta | A' \beta' \rangle = \langle V\beta | V\beta' \rangle$. Then we have $VA = A'$ by definition of V and $A = V^+ VA = V^+ A'$. These two equalities and their adjoints can be summarized in the following commutative diagram,

$$\begin{array}{ccccc} \mathbb{C}^{D^3} & \xrightarrow{A'} & \mathbb{C}^{d'} & & \\ A \downarrow & \nearrow V^+ & \searrow V & \downarrow A'^+ & \\ \mathbb{C}^d & & \mathbb{C}^{d'} & & \mathbb{C}^{D^3} \\ & & \searrow A^+ & & \end{array} \quad . \quad (\text{A.4})$$

Moreover, such V with $VA = A'$ is unique. Indeed, since A is surjective, any other V' with $V'A = A' = VA$ is equal to V .

Now, according to Eq. A.2 and taking the basic property of contraction as shown in Fig. A.1, we have $\mathbf{A}^+ \mathbf{A} = \text{Tr}_{\{\mathbb{C}^{2D}\}}[\mathbf{E} \otimes \mathbf{E} \otimes \mathbf{E}] = |\lambda|^2 \mathbf{E}$ as discussed in the previous

subsection. Replacing A' in Eq. A.4 by $(1/\lambda)\mathbf{A}$ and V by W , we can conclude that $WA = (1/\lambda)\mathbf{A}$, and hence we have

$$W^+ \text{Tr}_{\{\mathbb{C}^D\}}[A \otimes A \otimes A] = W^+ \mathbf{A} = \lambda A \quad (\text{A.5})$$

as desired. Obviously, $\text{Im}A = \text{Im}W$ according to Eq. A.4. We have recovered A with the coarse graining operator W . The coarse graining operator is uniquely determined by \mathbf{E} and its scale invariance. Indeed, if there is another W' with $\text{Im}A = W'$ and satisfying Eq. A.1, then $W'W'^+$ is the projection on $\text{Im}A$ and we have $W'A = (1/\lambda)\mathbf{A}$. Then since A is surjective, we have $W' = W$. Note that the commutative diagram in Eq. A.4 further implies that the tensors A and A' with $d' = d$ (guaranteeing that V is unitary) determine the same fixed-point state up to a local unitary operator of the form V^\otimes .

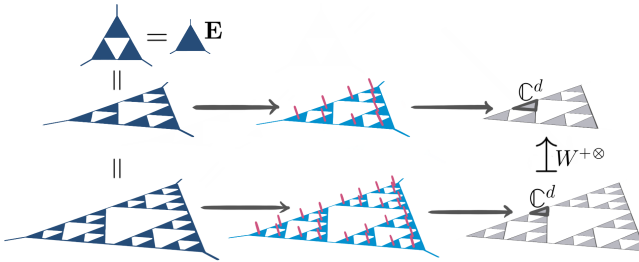


FIG. A.2. The framework of how \mathbf{E} and its scale invariance determines a fixed-point state and its self-similar patterns.

3. Discussion

Our coarse graining scheme is consistent to the one realized by Schmidt decomposition of \mathbf{A} as belonging to $(\mathbb{C}^d)^{\otimes 3} \otimes \mathbb{C}^{D^3}$ used in entanglement renormalization in 1D and 2D [26, 33]. Our framework is general and emphasizes that the coarse graining operator for a fixed point can be uniquely specified from the scale-invariance equation of transfer matrix. This framework can be illustrated in Fig. B: The zoom-in invariance of \mathbf{E} determines the tensor networks contracted from copies of A and hence the fixed-point states from smaller system size to larger system size; then the zoom-out invariance of \mathbf{E} as represented by the uniquely defined coarse graining maps fixed-point states from larger size back to smaller size. The three examples in the main text simply come from three transfer matrices as solutions to Eq. A.2. This way, we say that Fig. B endows fixed-point states with well-defined self-similarity in their entanglement.

Appendix B: Ergodicity of $T_{ii'}$'s

Following the discussion in the last paragraph of Sec. VI E, we prove that any $|\psi_m\rangle$ can be mapped to

$|\psi_{m_0}\rangle = |000\cdots\rangle$ by applying the $T_{ii'}$ operators finite times on different pairs of neighboring vertices (i, i') .

In this section we prove a more general condition which directly implies the desired condition. We consider a qudit-product-state $|\chi\rangle$ of the form $|\alpha\alpha'\alpha''\cdots\rangle$. For convenience in our proof, we reorganize the basis states in the qudit-product form as $|\alpha_1\alpha_2\alpha_3\rangle \otimes |\alpha\alpha'\alpha''\cdots\rangle$ where $\alpha_1, \alpha_2, \alpha_3$ stand for the single-qudit states on the three corner vertices while $\alpha\alpha'\alpha''\cdots$ stand for the rest. We still use the colored triangle to represent each $|\alpha\rangle$ as introduced in Sec. VI, and assume that $|\chi\rangle$ satisfies the same constraints (even number of red sides) on all circles but not on the lateral sides of the lattice.

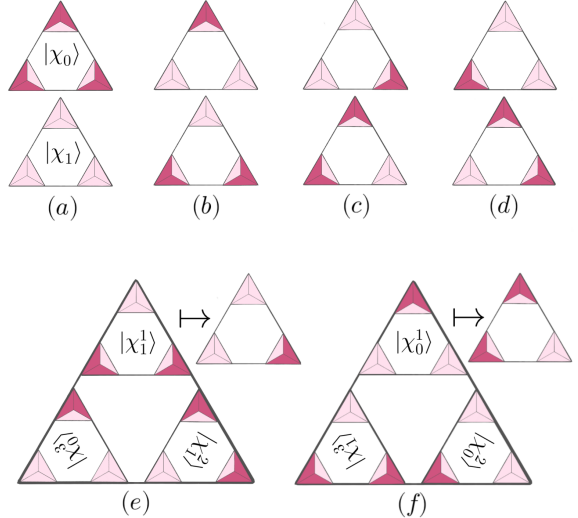


FIG. B.3. (a), (b), (c) and (d) are the four possible cases for $|\chi_0\rangle$ (upper) and $|\chi_1\rangle$ (lower). (e) and (f) are the two combinations $|\chi_1^1\rangle \otimes |\chi_1^2\rangle \otimes |\chi_0^3\rangle$ and $|\chi_0^1\rangle \otimes |\chi_0^2\rangle \otimes |\chi_1^3\rangle$ that $|\chi\rangle$ can be mapped to, in which each pair of neighboring qudits linking the big blocks is either in $|0\rangle \otimes |0\rangle$ or in $|1\rangle \otimes |1\rangle$. The two states are eventually mapped to the desired $|\chi_0\rangle$ and $|\chi_1\rangle$.

We want to prove the following condition: By applying the $T_{ii'}$ operators enough times on certain pairs of neighboring vertices (i, i') , $|\chi\rangle$ can be mapped to exactly two qudit-product-states $|\chi_0\rangle$ and $|\chi_1\rangle$ of the form $|\alpha_1\alpha_2\alpha_3\rangle \otimes |000\cdots\rangle$, i.e. with all qudits in $|0\rangle$ except for the three corners; Furthermore, $|\chi_0\rangle$ and $|\chi_1\rangle$ must be one of the four cases illustrated in Fig. B.3(a), B.3(b), B.3(c) and B.3(d) respectively where we omit the states $|000\cdots\rangle$ and only represent $|\alpha_1\alpha_2\alpha_3\rangle$ pictorially for simplicity.

We prove by induction on the system size, i.e. the finite generation of the Sierpiński lattice. It is trivial to prove that the condition holds for the smallest generation, i.e., when states are defined on a block. Now we assume that the condition is true for the n -th generation. We just need to prove that the condition holds for the $n+1$ -th generation.

Consider $|\chi\rangle$ on the lattice of the $n+1$ -th generation. Since $|\chi\rangle$ is a qudit-product-state, it can always be writ-

ten as $|\chi\rangle = |\chi^1\rangle \otimes |\chi^2\rangle \otimes |\chi^3\rangle$ where $|\chi^1\rangle$, $|\chi^2\rangle$ and $|\chi^3\rangle$ are the states on the three big triangular blocks which together form the whole lattice. Obviously, $|\chi^1\rangle$, $|\chi^2\rangle$ and $|\chi^3\rangle$ are on the lattice of the n -th generation, satisfying the constraints on all circles therein, and hence can be mapped to $|\chi_0^1\rangle$, $|\chi_1^1\rangle$, $|\chi_0^2\rangle$, $|\chi_1^2\rangle$ and $|\chi_0^3\rangle$, $|\chi_1^3\rangle$ respectively. In other words, by applying the $T_{ii'}$ operators enough times on certain pairs of neighboring vertices (i, i') , $|\chi\rangle$ can be mapped to the eight combination of the six states, i.e. $|\chi_0^1\rangle \otimes |\chi_0^2\rangle \otimes |\chi_0^3\rangle$, $|\chi_1^1\rangle \otimes |\chi_1^2\rangle \otimes |\chi_1^3\rangle$, ... Note that in any of such combination, there are even number of $|1\rangle$ on the six qudits connecting the three big blocks, since $|\chi\rangle$ satisfies the constraints (even number of red sides) on the largest circle. It can be easily shown that there are exactly two of such combinations, for example $|\chi_1^1\rangle \otimes |\chi_1^2\rangle \otimes |\chi_0^3\rangle$, $|\chi_0^1\rangle \otimes |\chi_0^2\rangle \otimes |\chi_1^3\rangle$, ... as il-

lustrated in Fig. B.3(e) and B.3(f) respectively, in which each pair of neighboring qudits linking the big blocks is either in $|0\rangle \otimes |0\rangle$ or in $|1\rangle \otimes |1\rangle$. Then, as shown in Fig. B.3(e) and B.3(f), applying the $T_{ii'}$ to those pairs in $|1\rangle \otimes |1\rangle$, $|\chi\rangle$ is eventually mapped to two states of the form $|\alpha_1\alpha_2\alpha_3\rangle \otimes |000\dots\rangle$. Furthermore, according to the four cases illustration in Fig. B.3(a), B.3(b), B.3(c) and B.3(d), the eventual two states are exactly within one of the four cases, and hence are the desired $|\chi_0\rangle$ and $|\chi_1\rangle$. Indeed, according to the constraints of $|\chi\rangle$ on the lateral sides, $|\chi_0\rangle$ and $|\chi_1\rangle$ and the only possible cases of the form $|\alpha_1\alpha_2\alpha_3\rangle \otimes |000\dots\rangle$. Therefore, the desired condition is proved.

Now, if we apply the condition to the case in Sec. VI E, it is obvious that any $|\psi_m\rangle$ can be mapped to $|\psi_{m_0}\rangle = |000\dots\rangle$ by applying the $T_{ii'}$ operators finite times on different pairs of neighboring vertices (i, i') .

[1] X.-G. Wen, Vacuum Degeneracy of Chiral Spin State in Compactified Spaces, *Phys. Rev. B* **40**, 7387 (1989).

[2] X.-G. Wen, Topological Orders in Rigid States, *Int. J. Mod. Phys. B* **4**, 239 (1990).

[3] X.-G. Wen and Q. Niu, Ground-State Degeneracy of the Fractional Quantum Hall States in the Presence of a Random Potential and on High-Genus Riemann Surfaces, *Phys. Rev. B* **41**, 9377 (1990).

[4] A. Y. Kitaev, Fault-tolerant quantum computation by anyons, *Ann. Phys. (N. Y.)* **303**, 2 (2003).

[5] M. H. Freedman, A. Kitaev, M. J. Larsen, and Z. H. Wang, Topological quantum computation, *Bull. Am. Math. Soc.* **40**, 31 (2003).

[6] J. Shang, Y. Wang, M. Chen, J. Dai, X. Zhou, J. Kuttner, G. Hilt, X. Shao, J. M. Gottfried, and K. Wu, Assembling molecular Sierpiński triangle fractals, *Nat. Chem.* **7**, 389 (2015).

[7] Y. Wang, S. Subhankar, P. Bienias, M. Łącki, T.-C. Tsui, M. A. Baranov, A. V. Gorshkov, P. Zoller, J. V. Porto, and S. L. Rolston, Dark State Optical Lattice with a Subwavelength Spatial Structure, *Phys. Rev. Lett.* **120**, 083601 (2018).

[8] S. N. Kempkes, M. R. Slot, S. E. Freeney, S. J. Zevenuhuizen, D. Vanmaekelbergh, I. Swart, and C. M. Smith, Design and characterization of electrons in a fractal geometry, *Nat. Phys.* **15**, 127 (2019).

[9] C. Liu, Y. Zhou, G. Wang, Y. Yin, C. Li, H. Huang, D. Guan, Y. Li, S. Wang, H. Zheng, C. Liu, Y. Han, J. W. Evans, F. Liu, and J. Jia, Sierpiński Structure and Electronic Topology in Bi Thin Films on InSb(111)B Surfaces, *Phys. Rev. Lett.* **126**, 176102 (2021).

[10] X. Y. Xu, X. W. Wang, D. Y. Chen, C. M. Smith, and X. M. Jin, Quantum transport in fractal networks, *Nat. Photonics* **15**, 703 (2021).

[11] M. Brzezińska, A. M. Cook, and T. Neupert, Topology in the Sierpiński-Hofstadter problem, *Phys. Rev. B* **98**, 205116 (2018).

[12] A. Agarwala, S. Pai, and V. B. Shenoy, Fractalized Metals, *arXiv:1803.01404* (2018).

[13] S. Pai and A. Prem, Topological states on fractal lattices, *Phys. Rev. B* **100**, 155135 (2019).

[14] M. Fremling, M. van Hooft, C. M. Smith, and L. Fritz, Existence of robust edge currents in Sierpiński fractals, *Phys. Rev. Res.* **2**, 013044 (2020).

[15] S. Manna, B. Pal, W. Wang, and A. E. B. Nielsen, Anyons and fractional quantum Hall effect in fractal dimensions, *Phys. Rev. Res.* **2**, 023401 (2020).

[16] A. A. Iliasov, M. I. Katsnelson, and S. Yuan, Hall conductivity of a Sierpiński carpet, *Phys. Rev. B* **101**, 045413 (2020).

[17] X. Yang, W. Zhou, P. Zhao, and S. Yuan, Confined electrons in effective plane fractals, *Phys. Rev. B* **102**, 245425 (2020).

[18] Z. Yang, E. Lustig, Y. Lumer, and M. Segev, Photonic Floquet topological insulators in a fractal lattice, *Light Sci. Appl.* **9**, 128 (2020).

[19] S. Manna, C. W. Duncan, C. A. Weidner, J. F. Sherson, and A. E. B. Nielsen, Laughlin-Type Topological Order on a Fractal Lattice with a Local Hamiltonian, *arXiv:2106.13816* (2021).

[20] S. Fischer, M. van Hooft, T. van der Meijden, C. M. Smith, L. Fritz, and M. Fremling, Robustness of chiral edge modes in fractal-like lattices below two dimensions: A case study, *Phys. Rev. Res.* **3**, 043103 (2021).

[21] S. Sarangi and A. E. B. Nielsen, Effect of coordination on topological phases on self-similar structures, *arXiv:2101.02723* (2021).

[22] H. Zou and W. Wang, Gapless Spin Liquid and Non-local Corner Excitation in the Spin-1/2 Heisenberg Antiferromagnet on Fractal, *arXiv:2105.12487* (2021).

[23] X. Li, M. C. Jha, and A. E. B. Nielsen, Laughlin topology on fractal lattices without area law entanglement, *arXiv:2201.04652* (2022).

[24] G. Zhu, T. Jochym-O'Connor, and A. Dua, Topological Order, Quantum Codes and Quantum Computation on Fractal Geometries, *arXiv:2108.00018* (2021).

[25] X. Chen, Z.-C. Gu, and X.-G. Wen, Local unitary transformation, long-range quantum entanglement, wave function renormalization, and topological order, *Phys. Rev. B* **82**, 155138 (2010).

[26] B. Zeng, X. Chen, D.-L. Zhou, and X.-G. Wen, *Quantum Information Meets Quantum Matter – From Quantum*

Entanglement to Topological Phase in Many-Body Systems (Springer, 2019).

[27] R. Moessner and S. L. Sondhi, Resonating valence bond phase in the triangular lattice quantum dimer model, *Phys. Rev. Lett.* **86**, 1881 (2001).

[28] M. A. Levin and X.-G. Wen, String-net condensation: A physical mechanism for topological phases, *Phys. Rev. B* **71**, 045110 (2005).

[29] A. Kitaev, Anyons in an exactly solved model and beyond, *Ann. Phys. (N. Y.)* **321**, 2 (2006).

[30] G. Semeghini, H. Levine, A. Keesling, S. Ebadi, T. T. Wang, D. Bluvstein, R. Verresen, H. Pichler, M. Kalinowski, R. Samajdar, A. Omran, S. Sachdev, A. Vishwanath, M. Greiner, V. Vuletić, and M. D. Lukin, Probing topological spin liquids on a programmable quantum simulator, *Science (80-.)* **374**, 1242 (2021).

[31] K. J. Satzinger, X. Mi, A. Dunsworth, C. Gidney, I. Aleiner, F. Arute, K. Arya, J. Atalaya, R. Babbush, J. C. Bardin, R. Barends, J. Basso, A. Bengtsson, A. Bilmes, M. Broughton, B. B. Buckley, D. A. Buell, B. Burkett, N. Bushnell, B. Chiaro, R. Collins, W. Courtney, S. Demura, A. R. Derk, D. Eppens, C. Erickson, L. Faoro, E. Farhi, A. G. Fowler, B. Foxen, M. Giustina, A. Greene, J. A. Gross, M. P. Harrigan, S. D. Harrington, J. Hilton, S. Hong, T. Huang, W. J. Huggins, L. B. Ioffe, S. V. Isakov, E. Jeffrey, Z. Jiang, D. Kafri, K. Kechedzhi, T. Khattar, S. Kim, P. V. Klimov, A. N. Korotkov, F. Kostritsa, D. Landhuis, P. Laptev, A. Locharla, E. Lucero, O. Martin, J. R. McClean, M. McEwen, K. C. Miao, M. Mohseni, S. Montazeri, W. Mruczkiewicz, J. Mutus, O. Naaman, M. Neeley, C. Neill, M. Y. Niu, T. E. O'Brien, A. Opremcak, B. Pató, A. Petukhov, N. C. Rubin, D. Sank, V. Shvarts, D. Strain, M. Szalay, B. Villalonga, T. C. White, Z. Yao, P. Yeh, J. Yoo, A. Zalcman, H. Neven, S. Boixo, A. Megrant, Y. Chen, J. Kelly, V. Smelyanskiy, A. Kitaev, M. Knap, F. Pollmann, and P. Roushan, Realizing topologically ordered states on a quantum processor, *Science (80-.)* **374**, 1237 (2021).

[32] Our example of fixed-point states are all equal-weight sum of qudit-product-states satisfying certain constraints. In these cases, entanglement patterns can be understood as the pictorial representations of the constraints. Indeed, such constraints comprehensively characterize correlation and entanglement in states.

[33] F. Verstraete, J. I. Cirac, J. I. Latorre, E. Rico, and M. M. Wolf, Renormalization-group transformations on quantum states., *Phys. Rev. Lett.* **94**, 140601 (2005).

[34] G. Vidal, Entanglement Renormalization: an introduction, in *Underst. Quantum Phase Transitions* (CRC Press, 2010) Chap. 5, arXiv:0912.1651.

[35] A. Kitaev and J. Preskill, Topological entanglement entropy, *Phys. Rev. Lett.* **96**, 110404 (2006).

[36] M. Levin and X. G. Wen, Detecting topological order in a ground state wave function, *Phys. Rev. Lett.* **96**, 110405 (2006).

[37] A. Erhard, H. Poulsen Nautrup, M. Meth, L. Postler, R. Stricker, M. Stadler, V. Negnevitsky, M. Ringbauer, P. Schindler, H. J. Briegel, R. Blatt, N. Friis, and T. Monz, Entangling logical qubits with lattice surgery, *Nature* **589**, 220 (2021).

[38] A. Rahmani, K. J. Sung, H. Putterman, P. Roushan, P. Ghaemi, and Z. Jiang, Creating and Manipulating a Laughlin-Type $\nu = 1/3$ Fractional Quantum Hall State on a Quantum Computer with Linear Depth Circuits , *PRX Quantum* **1**, 020309 (2020).

[39] S. Bravyi, M. B. Hastings, and F. Verstraete, Lieb-robinson bounds and the generation of correlations and topological quantum order, *Phys. Rev. Lett.* **97**, 050401 (2006).

[40] M. P. Zaletel, R. S. K. Mong, F. Pollmann, and E. H. Rezayi, Infinite density matrix renormalization group for multicomponent quantum Hall systems, *Phys. Rev. B* **91**, 045115 (2015).

[41] J. Osorio Iregui, M. Troyer, and P. Corboz, Infinite matrix product states versus infinite projected entangled-pair states on the cylinder: A comparative study, *Phys. Rev. B* **96**, 115113 (2017).

[42] J.-Y. Chen, L. Vanderstraeten, S. Capponi, and D. Poilblanc, Non-Abelian chiral spin liquid in a quantum anti-ferromagnet revealed by an iPEPS study, *Phys. Rev. B* **98**, 184409 (2018).

[43] Here we view A as a linear map $A : \mathbb{C}^{3D} \rightarrow \mathbb{C}^d$ which is equivalent to A as a tensor in $\mathbb{C}^d \otimes \mathbb{C}^{3D}$.

[44] C. Weitenberg, M. Endres, J. F. Sherson, M. Cheneau, P. Schau, T. Fukuhara, I. Bloch, and S. Kuhr, Single-spin addressing in an atomic Mott insulator, *Nature* **471**, 319 (2011).

[45] Y. Yanay, J. Braumüller, S. Gustavsson, W. D. Oliver, and C. Tahan, Two-dimensional hard-core Bose-Hubbard model with superconducting qubits, *npj Quantum Inf.* **6**, 58 (2020).

[46] At finite system size we set $N^1/(N-3) = 1/2$ as if we exclude the three vertices at the corners since they are not covered by the interaction in H . This way, when system size increase to infinity as in thermodynamic limit, we exactly have $N^1/N = 1/2$.

[47] I. Affleck, T. Kennedy, E. H. Lieb, and H. Tasaki, Rigorous results on valence-bond ground states in antiferromagnets, *Phys. Rev. Lett.* **59**, 799 (1987).

[48] Using the operator defined in the next subsection, $T_{ii'} = S_i^1 S_{i'}^1$ for (i, i') connecting two neighboring blocks; $T_{ii'} = S_i^2 S_{i'}^3$ or $T_{ii'} = S_i^3 S_{i'}^2$ for (i, i') in the same block.

[49] In a connected graph, the distance between two vertices is the length of, i.e. the number of edges (links) in the shortest path connecting the two vertices. The diameter of a connected subset in a graph is the diameter of the subgraph induced by the subset, i.e., the maximal length of the shortest path within the subset which connects a pair of vertices in the subset.

[50] To be consistent with the case in 2D, a local patch of unitary operator of size P in the quantum circuit is defined as a unitary operator supported on a connected subset with diameter P , i.e. it acts as the identity operator on qudits outside the support. The P here confines the distance between any pair of vertices within the subset so that the unitary operator acts locally. Then, starting from a single vertex j as the support of O_j , the first layer of non-overlapping local unitary operators extends the size of the support at most by P since only one local patch contains j . And each of the following layers extends the support by $2P$ since the distance of the farthest apart vertex pair is extended at most by $2P$. Note that the layer structure in the quantum circuit guarantees the connectivity of J .

[51] N. Delfosse, P. Iyer, and D. Poulin, Generalized surface codes and packing of logical qubits, arXiv:1606.07116 (2016).

[52] W. Wang, V. Penna, and B. Capogrosso-Sansone, Analysis and resolution of the ground-state degeneracy of the two-component Bose-Hubbard model, [Phys. Rev. E **90**, 022116 \(2014\)](#).